Supporting Information

for

Comparing the reactivity of isomeric phosphinoferrocene nitrile and isocyanide in Pd(II) complexes: Synthesis of simple coordination compounds *vs*. preparation of P-chelated insertion products and Fischer-type carbenes

*Karel Škoch, Ivana Císařová, Filip Uhlík and Petr Štěpnička**

Contents

Additional structural diagrams

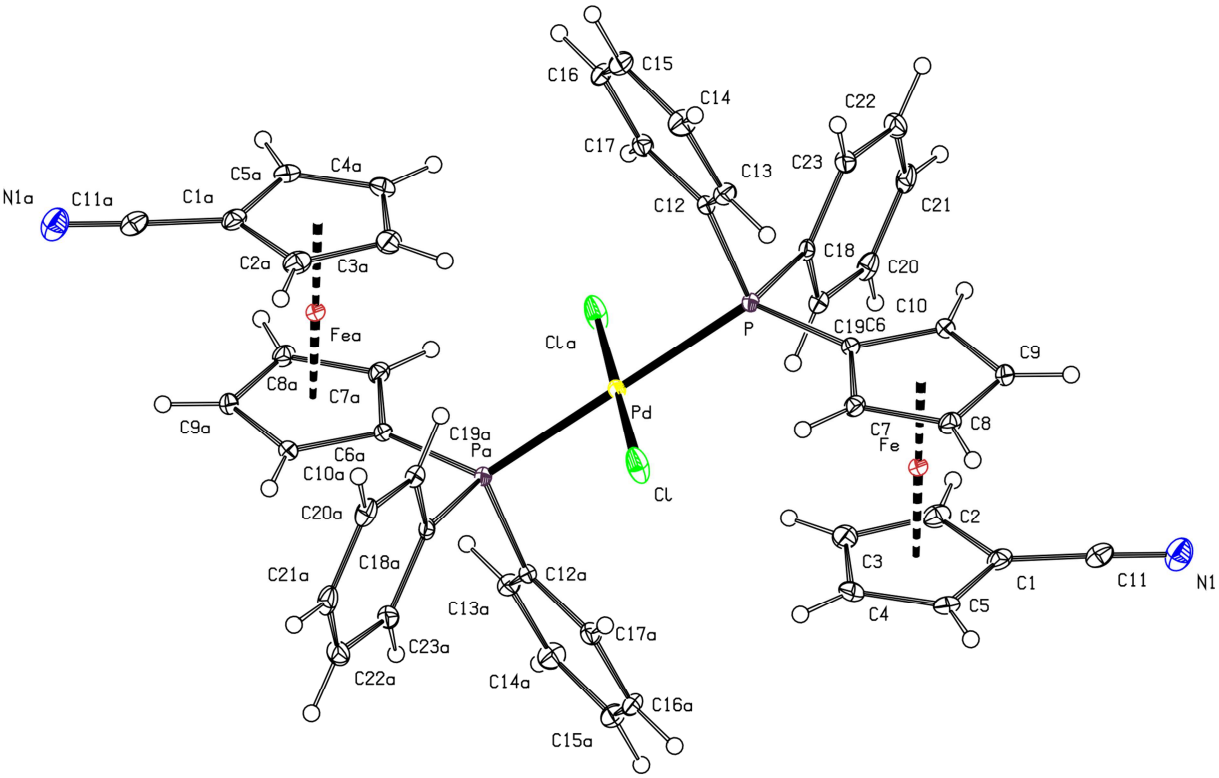

Figure S1. PLATON plot of the molecular structure of **7** (30% probability ellipsoids).

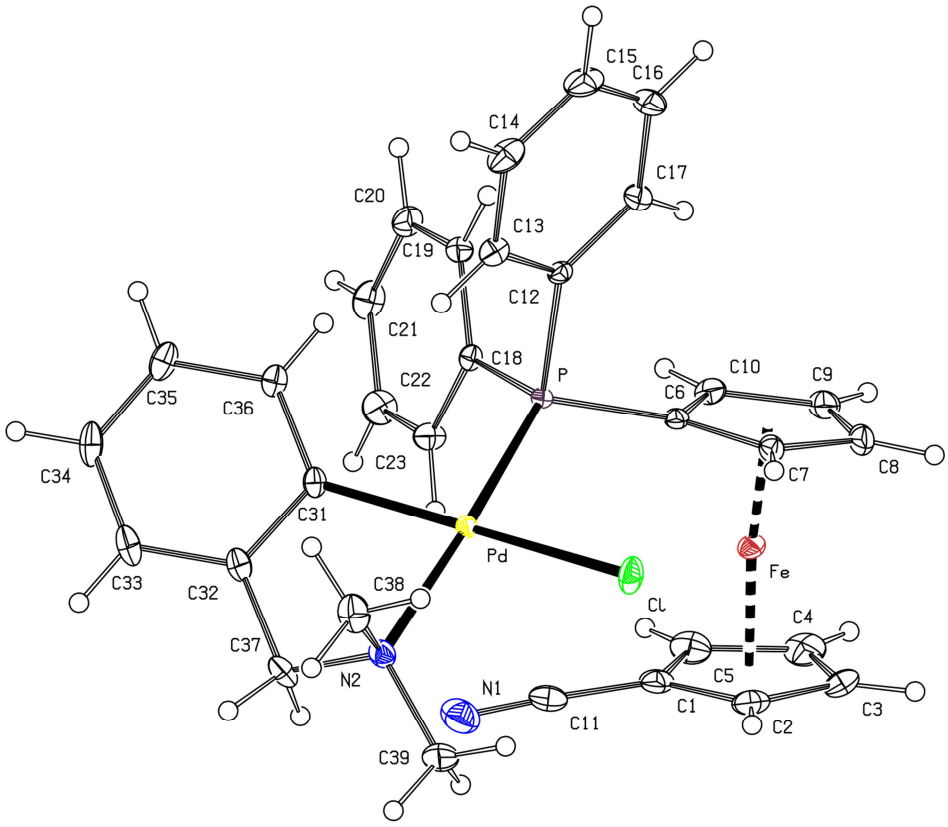

Figure S2. PLATON plot of the molecular structure of **8** (30% probability ellipsoids).

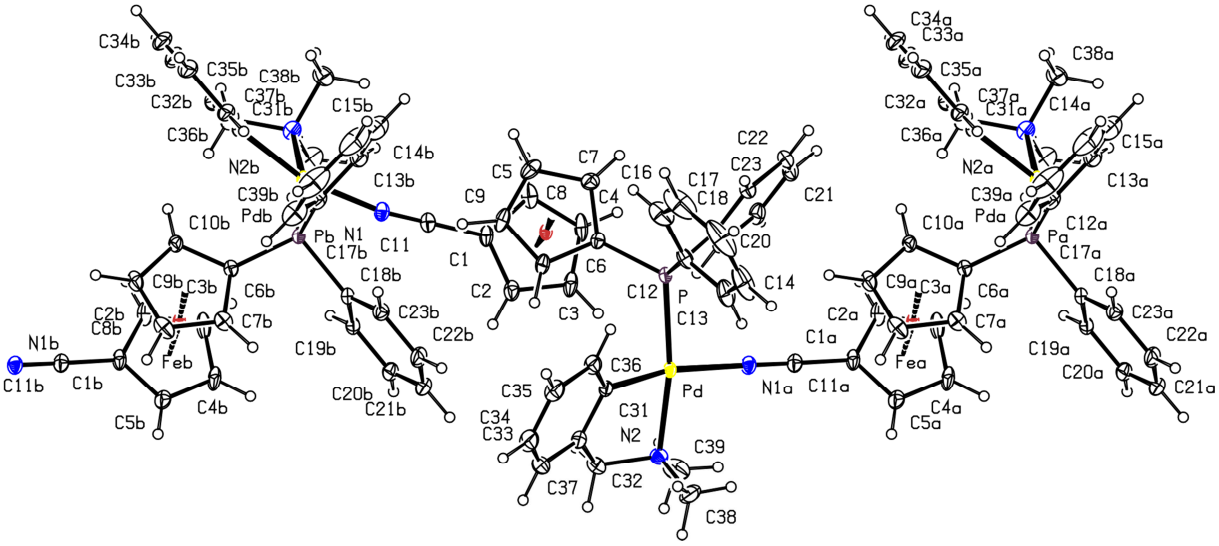

Figure S3. PLATON plot of the polymeric assembly in **9**·2$CHCl_3$ (30% probability ellipsoids).

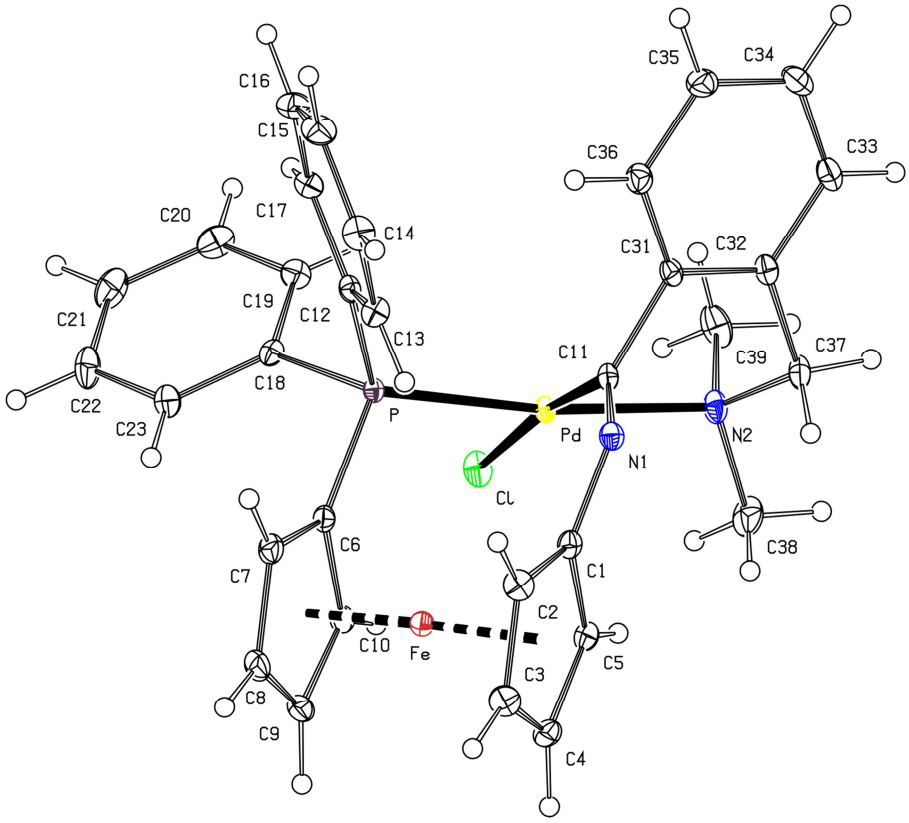

Figure S4. PLATON plot of the molecular structure of **10** (30% probability ellipsoids).

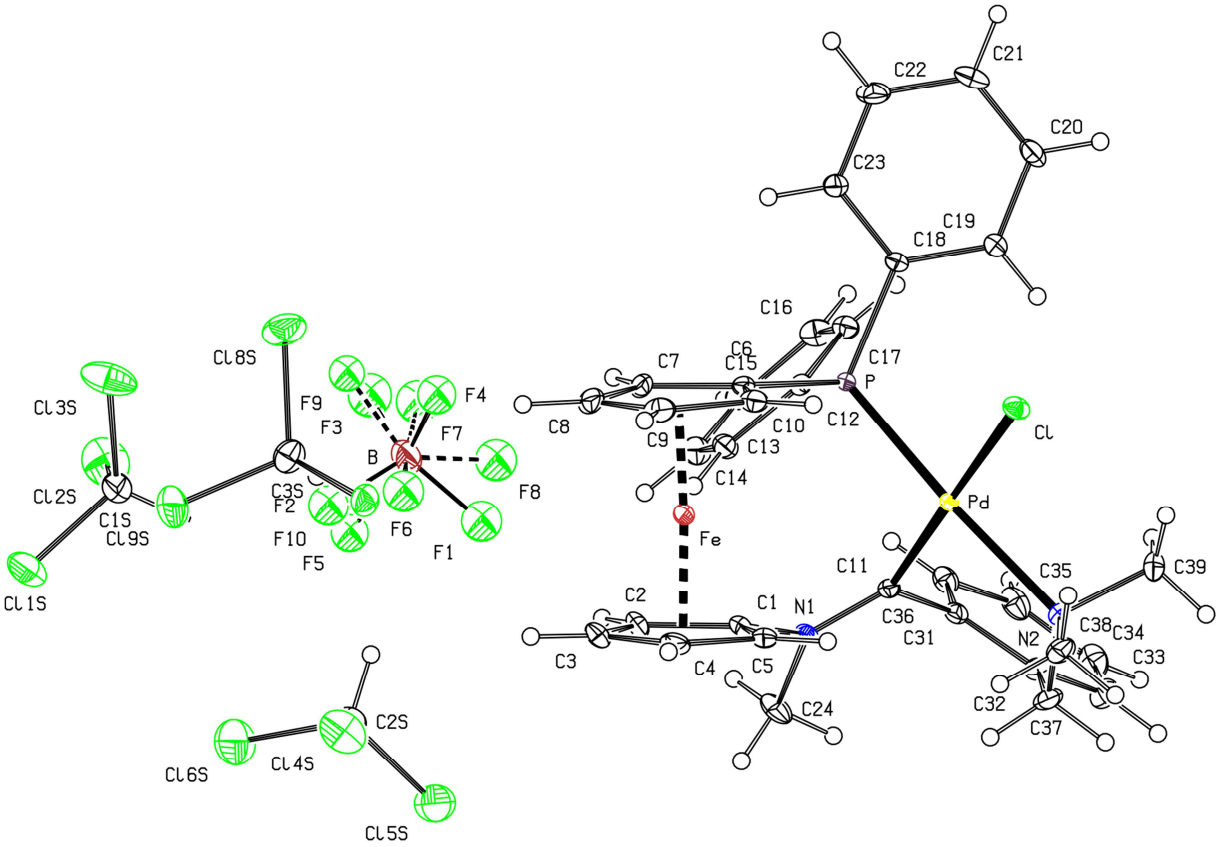

Figure S5. PLATON plot of the molecular structure of **11**·3$CHCl_3$ (30% probability ellipsoids).

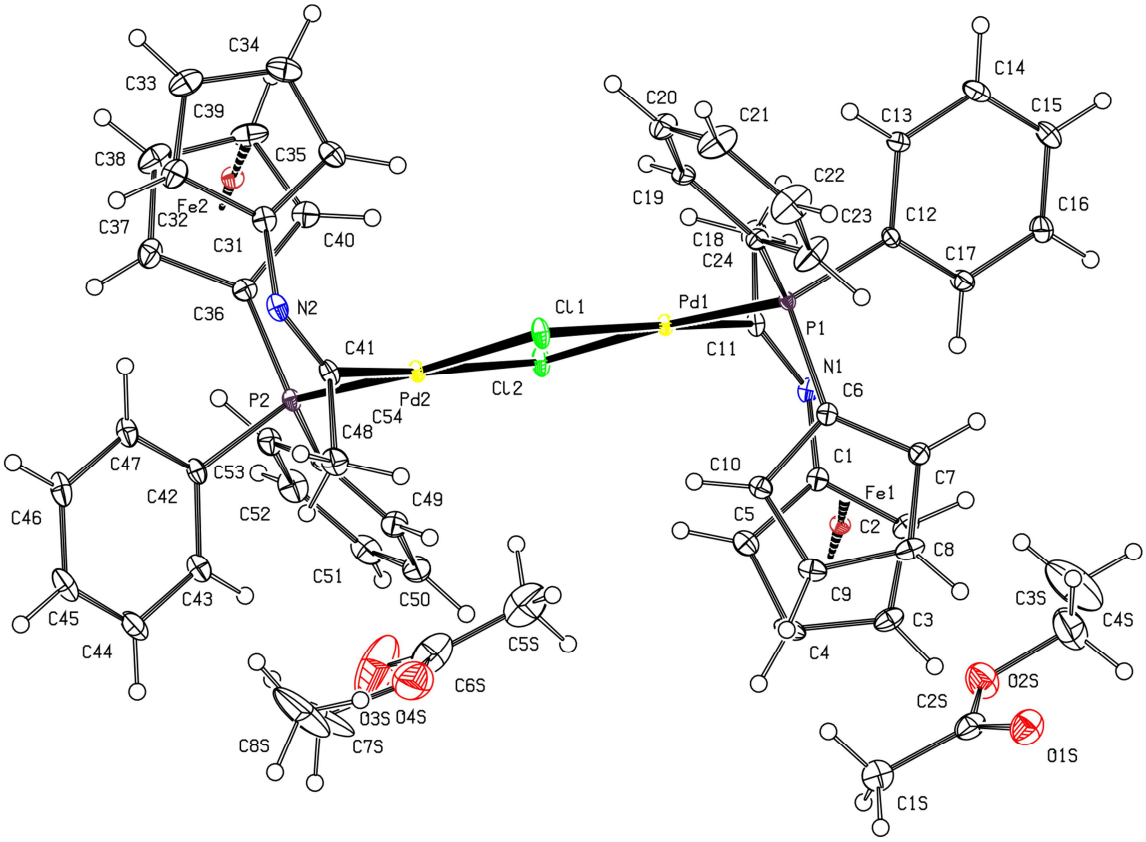

Figure S6. PLATON plot of the molecular structure of **12**·2AcOEt (30% probability ellipsoids).

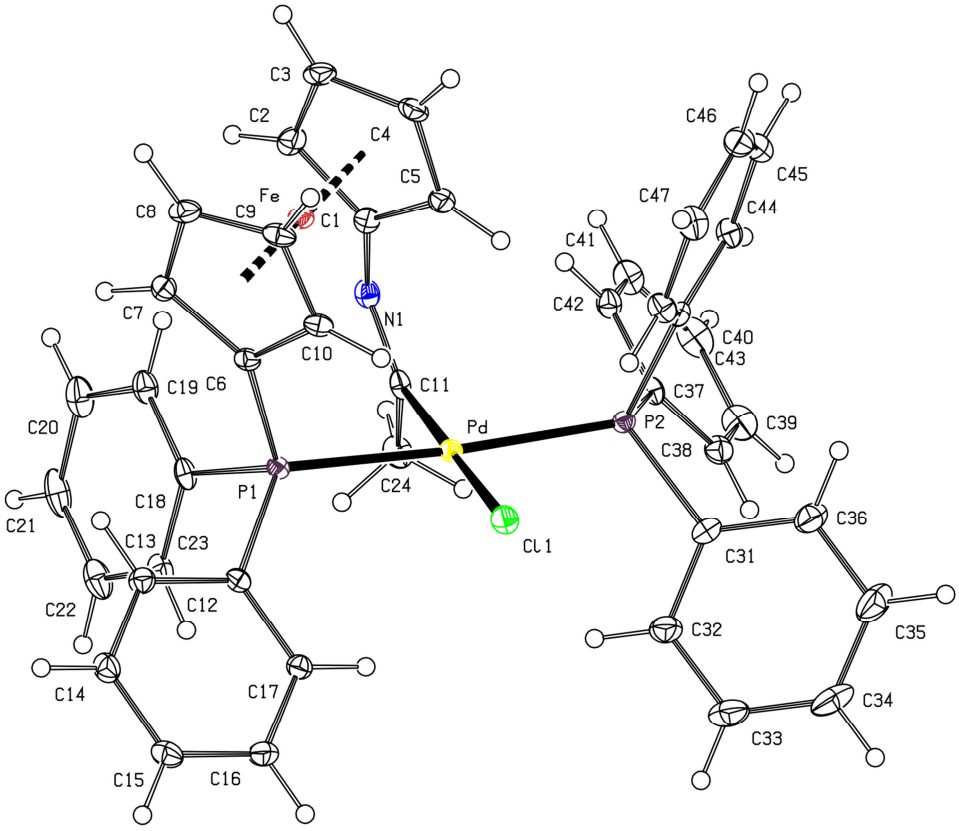

Figure S7. PLATON plot of the molecular structure of **13** (30% probability ellipsoids).

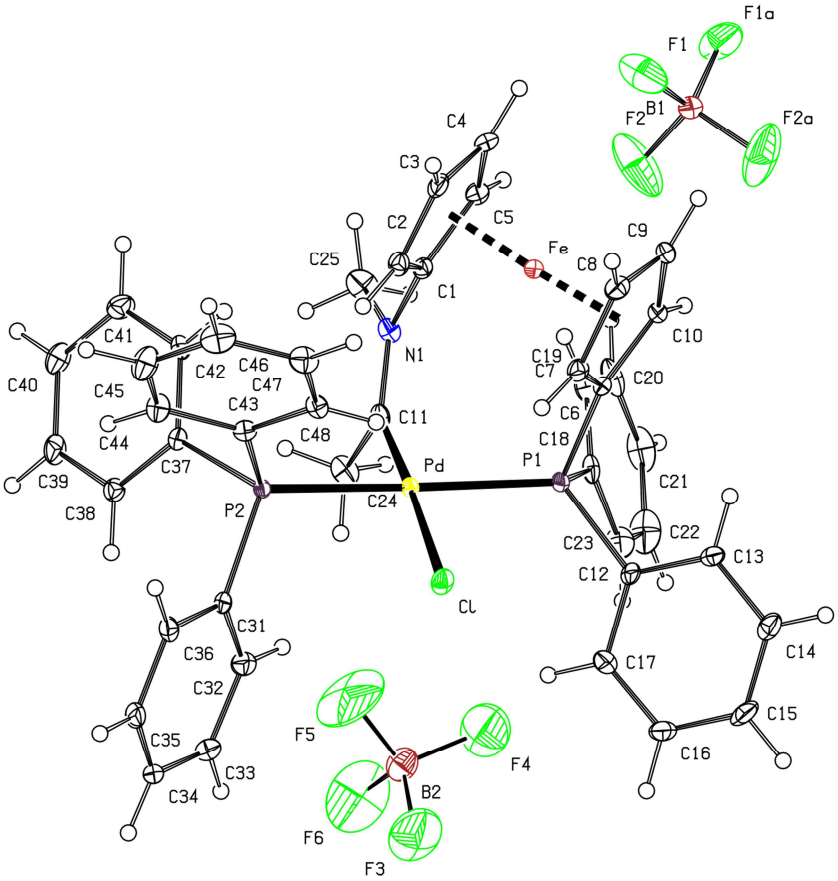

Figure S8. PLATON plot of the molecular structure of **14** (30% probability ellipsoids). Note that tthe anions reside over symmetry elements.

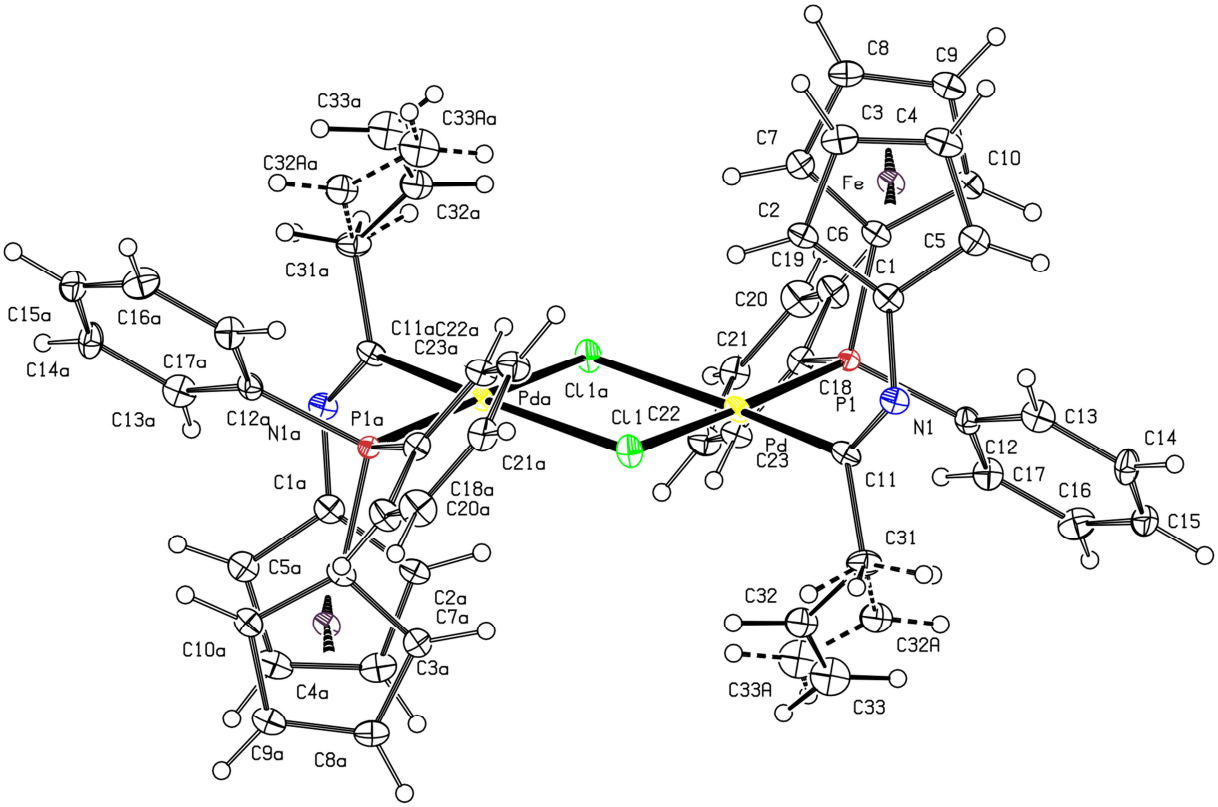

Figure S9. PLATON plot of the molecular structure of **15**·2$CHCl_3$ (30% probability ellipsoids). The solvent molecules are omitted for clarity.

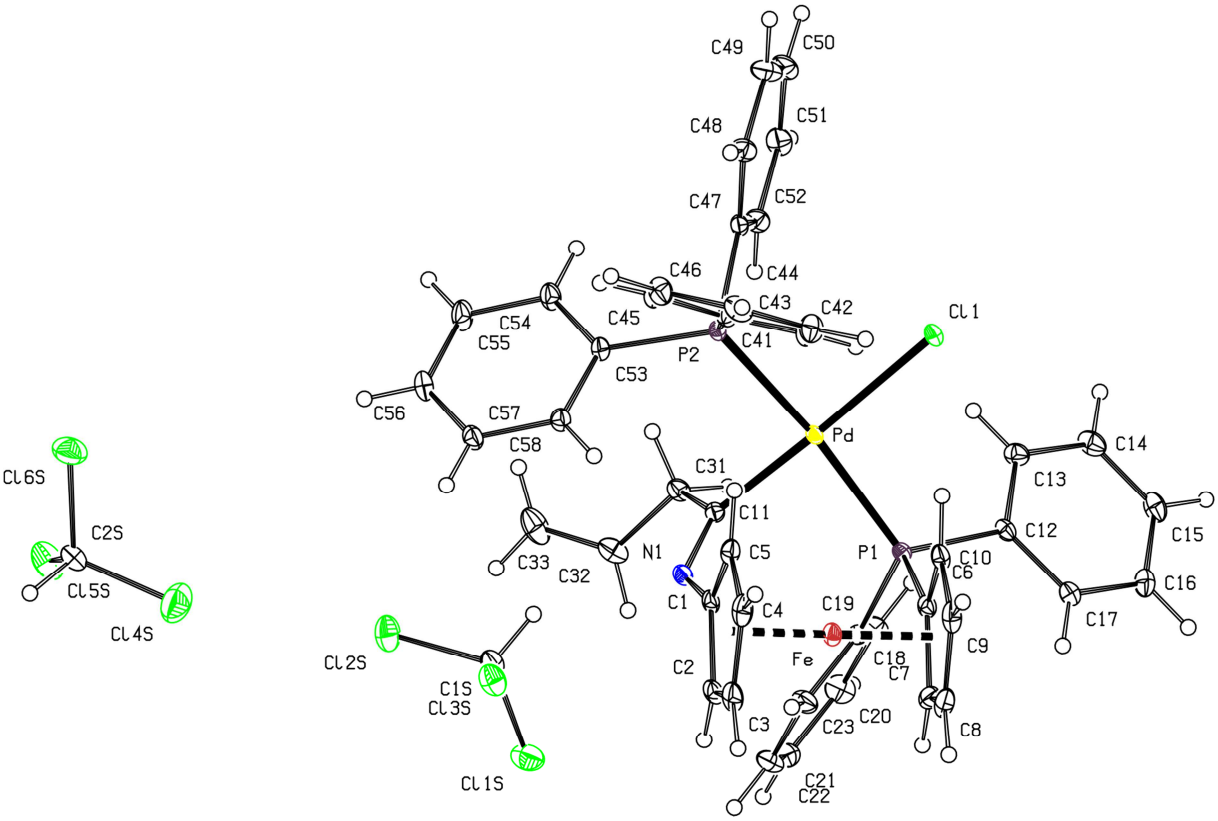

Figure S10. PLATON plot of the molecular structure of **16**·2$CHCl_3$ (30% probability ellipsoids).

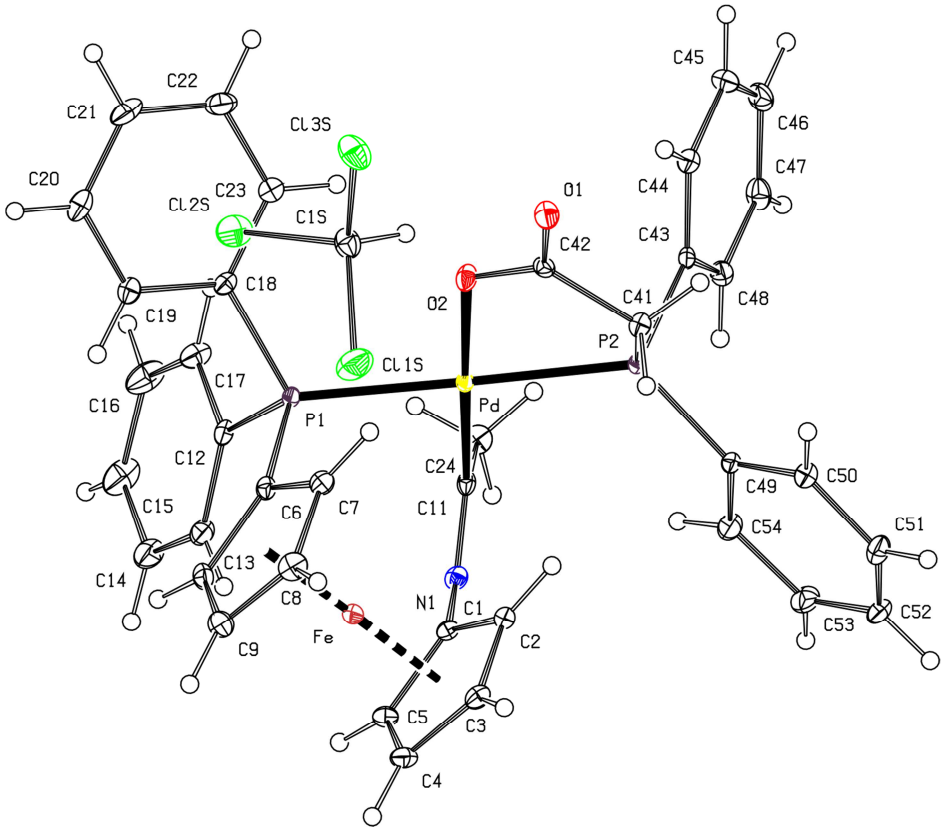

Figure S11. PLATON plot of the molecular structure of **19**·$CHCl_3$ (30% probability ellipsoids).

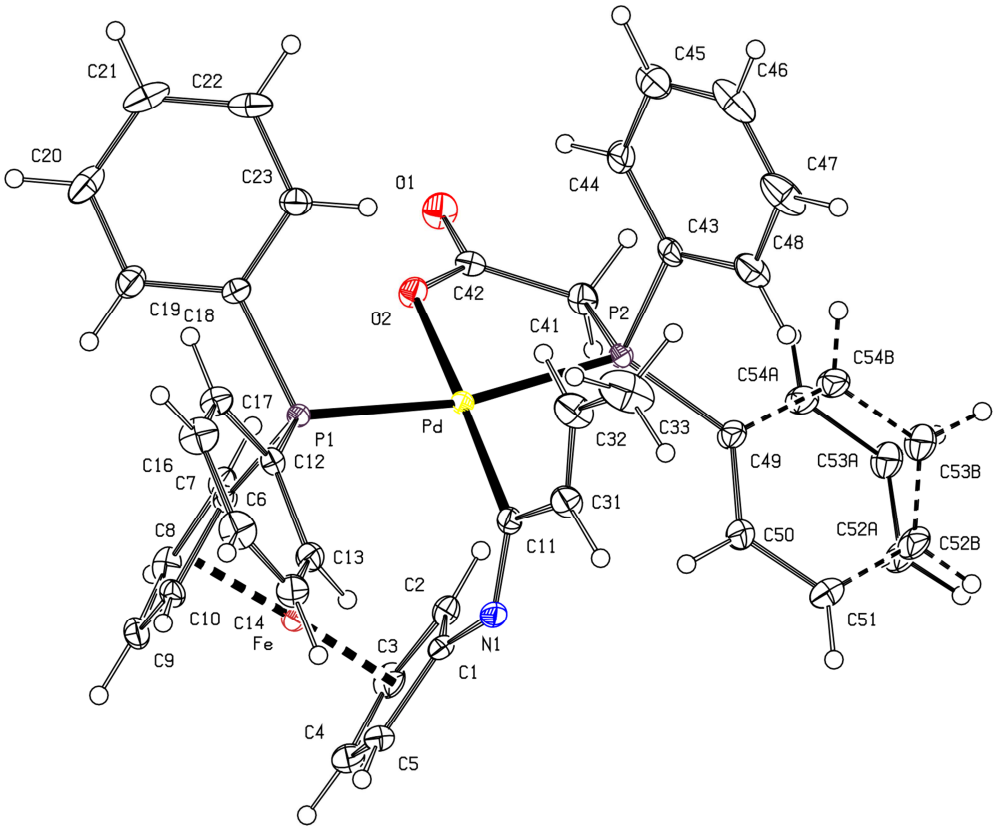

Figure S12. PLATON plot of the molecular structure of **20**·H_2O·1.5AcOEt (30% probability ellipsoids). The water molecule is omitted to avoid complicating the Figure.

Summary of crystallographic data and details on structure refinement

Details on structure refinement

Full-set diffraction data ($\pm h \pm k \pm l$, θ_{max} = 26.0 or 27.5°, data completeness > 99%) were collected at 120(2) K or 150(2) K using either Nonius KappaCCD diffractometer with a Bruker Apex-II image plate detector (compounds **7** and **8**) or a Bruker D8 VENTURE Kappa Duo PHOTON100 instrument with a IμS micro-focus X-ray tube (all other compounds), both equipped with a Cryostream Cooler (Oxford Cryosystems). Mo Kα radiation was used in all cases.

The structures were solved by direct methods (SHELXT)[1] and then refined by a full-matrix least squares routine based on F^2 using SHELXL-97.[2] The non-hydrogen atoms were refined with anisotropic displacement parameters. Hydrogen atoms were included in their calculated positions and refined using the "riding model" with U_{iso}(H) se to a multiple of U_{eq} of their bonding atom. Hydrogens on the solvating water molecules in **20**·H_2O·1.5AcOEt were identified on the difference electron density map and refined similarly (riding atoms).

Compound **12**·2AcOEt crystallized as a racemic twin (space group *Cc*). Contributions of the two enantiomeric domains were refined to 74:36. The solvating ethyl acetate in the structure of **20**·H_2O·1.5AcOEt was disordered and, hence, was modelled as diffuse electron density by PLATON SQUEEZE.[3] In addition, the water molecule and one phenyl ring in this structure had to be refined over two positions. Also disordered were the tetrafluoroborate anions in the structures of **11**·3$CHCl_3$ and **14** (in the latter case, the asymmetric unit contained two independent cation residing over symmetry elements of which one had to be refined over two positions), one solvent molecule in the structure of **9**·2$CHCl_3$ and, finally, the allyl moiety in the structure of **15**·2$CHCl_3$, which also was refined over two positions (69:31 ratio).

Relevant crystallographic data, data collection and structure refinement parameters are presented in Table S1. All geometric calculations were performed with a recent version of the PLATON program,[4] which was also used to prepare the structural diagrams.

Table S1. Selected crystallographic data and structure refinement parameters.

Compound	**7**	**8**	**9**·2$CHCl_3$
Formula	$C_{46}H_{36}Cl_2Fe_2N_2P_2Pd$	$C_{32}H_{30}ClFeN_2PPd$	$C_{34}H_{32}Cl_6F_6FeN_2PPdSb$
M	967.71	671.25	1109.28
Crystal system	triclinic	monoclinic	orthorhombic
Space group	P–1 (no. 2)	$P2_1/n$ (no. 14)	$Pbca$ (no. 61)
T/K	150(2)	150(2)	150(2)
a/Å	8.9445(4)	13.9367(5)	15.4514(6)
b/Å	10.0660(4)	11.4282(4)	17.2509(5)
c/Å	11.2913(4)	18.0078(6)	30.4720(9)
α/deg	82.150(2)		
β/deg	74.759(2)	100.323(1)	
γ/deg	85.368(2)		
V/Å^3	970.60(7)	2821.7(2)	8122.3(5)
Z	1	4	8
μ(Mo Kα)/mm^{-1}	1.453	1.327	1.941
Diffrns collected	14623	25368	88809
Independent diffrns	4468	6479	9367
Observed diffrns[a]	3791	5669	7878
R_{int}[b]/%	2.56	2.12	3.41
No. of parameters	250	345	475
R[c] obsd diffrns/%	2.90	2.20	2.94
R, wR[c] all data /%	3.96, 6.07	2.78, 5.07	4.04, 6.95
Δρ/e Å^{-3}	1.09, –0.73	0.75, –0.51	1.12, –1.03
CCDC entry	1857561	1857562	1857563

[a] Diffractions with $I > 2\sigma(I)$. [b] Definitions: $R_{int} = \Sigma|F_o^2 - F_o^2(\text{mean})|/\Sigma F_o^2$, where F_o^2(mean) denotes the average intensity of symmetry-equivalent diffractions. [c] $R = \Sigma||F_o| - |F_c||/\Sigma|F_o|$, w$R = [\Sigma\{w(F_o^2 - F_c^2)_2\}/\Sigma w(F_o^2)_2]^{½}$.

Table S1 continued

Compound	**10**	**11**·3$CHCl_3$	**12**·2AcOEt
Formula	$C_{32}H_{30}ClFeN_2PPd$	$C_{36}H_{36}BCl_{10}F_4FeN_2PPd$	$C_{56}H_{58}Cl_2Fe_2N_2O_4P_2Pd$
M	671.25	1131.20	1280.38
Crystal system	monoclinic	triclinic	monoclinic
Space group	$P2_1/c$ (no. 14)	$P\bar{1}$ (no. 2)	Cc (no. 9)
T/K	150(2)	150(2)	150(2)
a/Å	15.3228(5)	10.3024(5)	10.0527(4)
b/Å	9.4826(3)	12.6061(6)	19.7030(7)
c/Å	19.3688(6)	17.2042(8)	26.773(1)
α/deg		94.486(2)	
β/deg	97.717(1)	92.885(2)	98.947(2)
γ/deg		97.209(2)	
V/Å^3	2788.8(2)	2205.8(2)	5238.3(4)
Z	4	2	4
μ(Mo Kα)/mm^{-1}	1.343	1.426	1.430
Diffrns collected	58921	61027	62544
Independent diffrns	6417	10120	11983
Observed diffrns[a]	5850	9679	11672
R_{int}[b]/%	2.81	1.94	2.39
No. of parameters	345	513	638
R[c] obsd diffrns/%	2.01	3.26	2.17
R, wR[c] all data /%	2.37, 5.29	3.39, 8.00	2.28, 5.52
Δρ/e Å^{-3}	0.36, –0.66	1.30, –1.02	0.97, –0.55
CCDC entry	1857564	1857565	1857566

Table S1 continued

Compound	**13**	**14**	**15**·2$CHCl_3$
Formula	$C_{42}H_{36}ClFeNP_2Pd$	$C_{43}H_{39}BClF_4FeNP_2Pd$	$C_{54}H_{48}Cl_8Fe_2N_2P_2Pd_2$
M	814.36	916.20	1394.98
Crystal system	monoclinic	monoclinic	triclinic
Space group	$P2_1/n$ (no. 14)	$C2/c$ (no. 15)	$P\bar{1}$ (no. 2)
T/K	120(2)	150(2)	150(2)
a/Å	9.9066(3)	25.632(1)	9.4504(7)
b/Å	29.956(1)	19.4838(8)	10.7329(8)
c/Å	11.6226(4)	16.5874(7)	15.278(1)
α/deg			99.123(3)
β/deg	90.081(1)	112.617(2)	103.877(3)
γ/deg			112.080(2)
V/Å^3	3449.1(2)	7646.9(6)	1339.8(2)
Z	4	8	1
μ(Mo Kα)/mm^{-1}	1.145	1.057	1.689
Diffrns collected	30733	39837	24341
Independent diffrns	6782	7513	5287
Observed diffrns[a]	5698	5594	4273
R_{int}[b]/%	3.85	7.95	5.67
No. of parameters	434	503	587
R[c] obsd diffrns/%	2.87	3.93	4.39
R, wR[c] all data /%	3.98, 6.60	6.67, 8.01	6.12, 10.6
Δρ/e Å^{-3}	0.81, –0.56	0.73, –0.61	1.49, –1.21
CCDC entry	1857567	1857568	1857569

Table S1 continued

Compound	**16**·2$CHCl_3$	**19**·$CHCl_3$	**20**·H_2O·1.5AcOEt
Formula	$C_{46}H_{40}Cl_7FeNP_2Pd$	$C_{39}H_{34}Cl_3FeNO_2P_2Pd$	$C_{46}H_{49}FeNO_6P_2Pd$
M	1079.13	879.21	936.05
Crystal system	triclinic	Monoclinic	triclinic
Space group	P–1 (no. 2)	$P2_1/n$ (no. 14)	P–1 (no. 2)
T/K	120(2)	120(2)	150(2)
a/Å	11.9324(5)	17.2257(6)	9.7665(3)
b/Å	14.1508(7)	10.2128(3)	11.6683(4)
c/Å	15.7966(7)	21.7891(8)	17.5540(7)
α/deg	108.821(2)		84.011(2)
β/deg	101.045(2)	110.493(1)	82.117(1)
γ/deg	109.240(2)		77.953(1)
V/Å^3	2247.3(2)	3590.6(2)	1932.0(1)
Z	2	4	2
μ(Mo Kα)/mm^{-1}	1.245	1.254	0.978
Diffrns collected	88114	52455	34617
Independent diffrns	10343	8253	8879
Observed diffrns[a]	9358	7575	7843
R_{int}[b]/%	3.02	3.10	2.87
No. of parameters	523	443	448
R[c] obsd diffrns/%	2.47	2.27	2.57
R, wR[c] all data /%	2.96, 6.02	2.54, 5.82	3.20, 6.16
Δρ/e Å^{-3}	1.08, –0.73	0.46, –0.80	0.80, –0.75
CCDC entry	1857570	1857571	1857572

M	HOMO	LUMO	ρ(M) – ρ(M⁺)
13	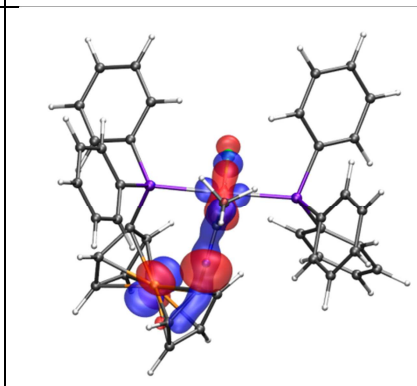	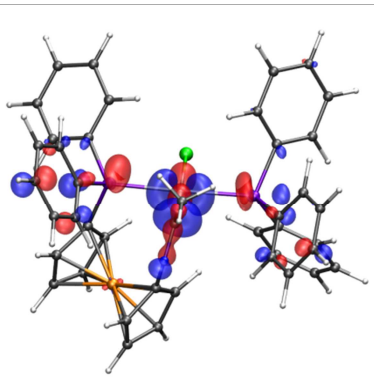	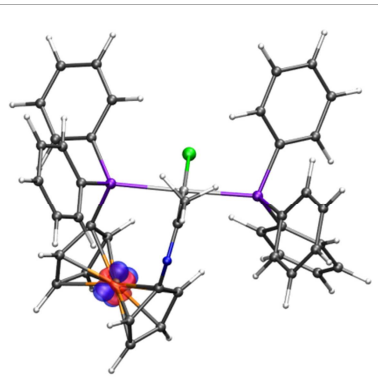
14	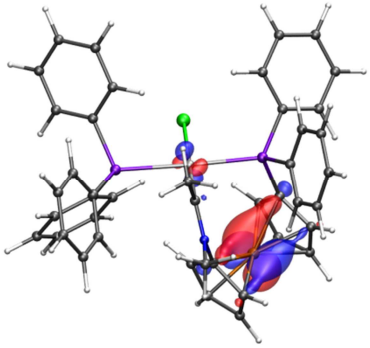	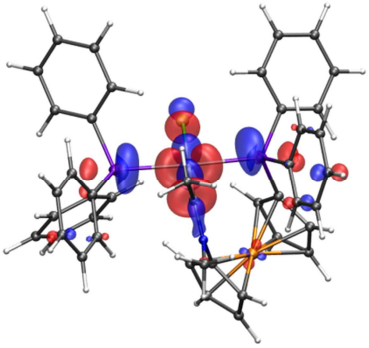	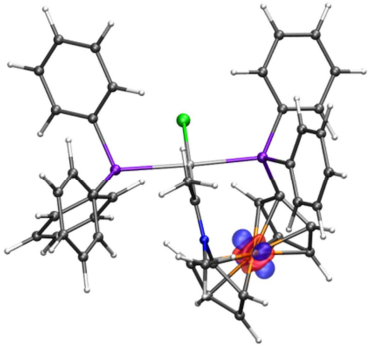

Figure 13. HOMO and LUMO orbitals (contour maps with isosufraces at ±0.05 a.u) and electron density difference contour maps ρ(M) – ρ(M⁺) at the geometry of M (isosufraces at ±0.02 a.u.) for compounds **13** and **14**.

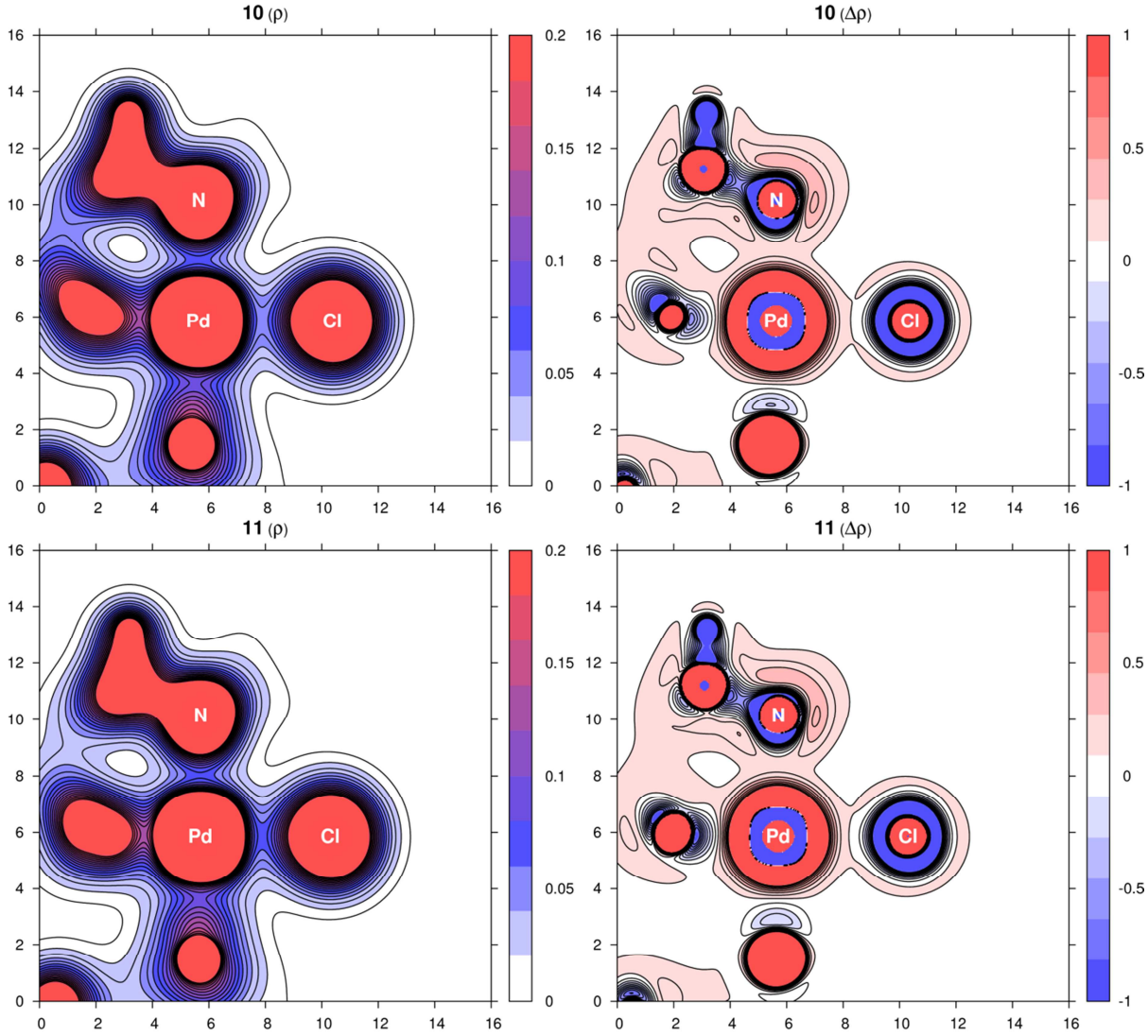

Figure 14. Electron density maps (ρ) and their Laplacians (Δρ) in planes defined by the palladium and the directly bonded N and Cl atoms for compounds **10** and **11**.

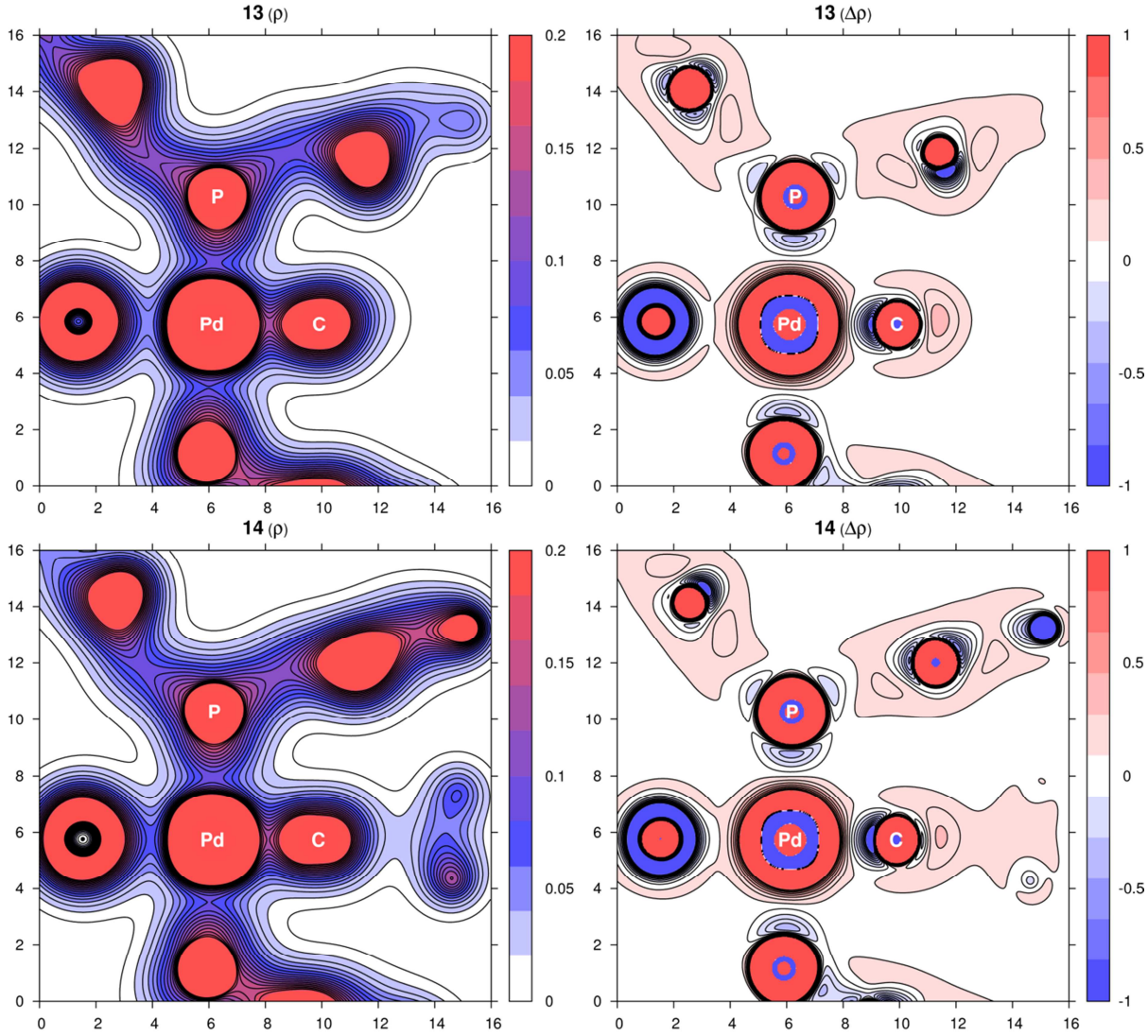

Figure 15. Electron density maps (ρ) and their Laplacians (Δρ) in planes defined by the palladium and the directly bonded P (ferrocene) and C atoms for compounds **13** and **14**.

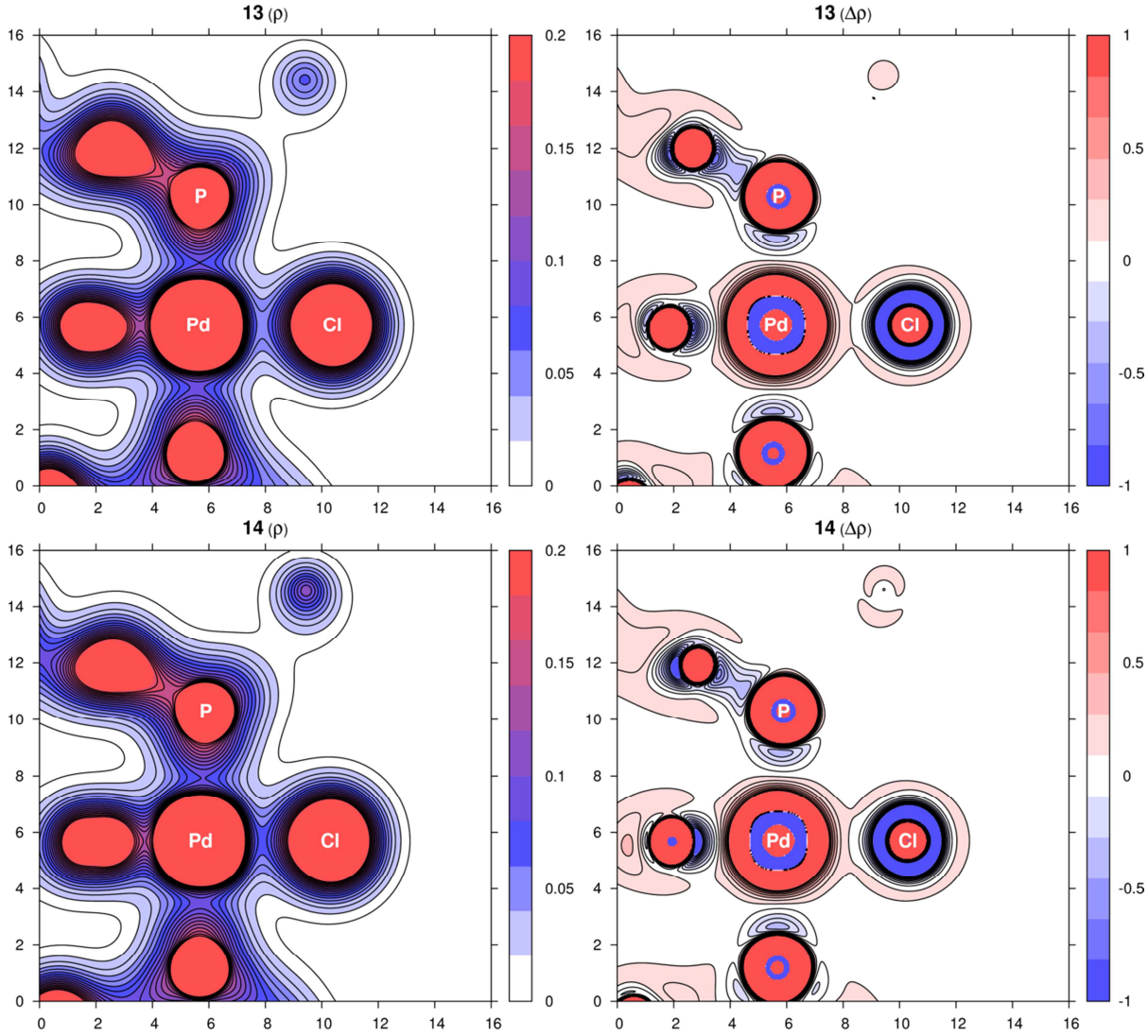

Figure 16. Electron density maps (ρ) and their Laplacians (Δρ) in planes defined by the palladium and the directly bonded P (PPh_3) and Cl atoms for compounds **13** and **14**.

UV-vis spectra of 10 and 11

The UV-vis spectra of **10** and **11** were recorded on UNICAM UV 300 spectrometer using 0.10 mM solutions in dichloromethane and 1 cm optical path (Figure S17).

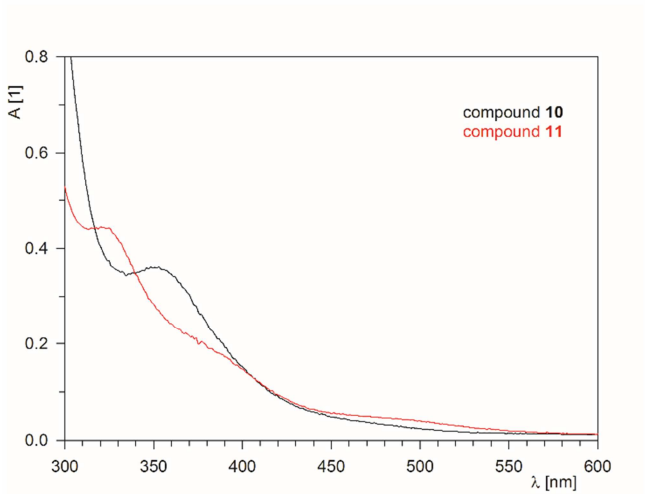

Figure S17. UV-vis spectra of **10** and **11** (0.10 mM solutions in CH_2Cl_2, optical path: 1.0 cm)

Copies of the NMR spectra

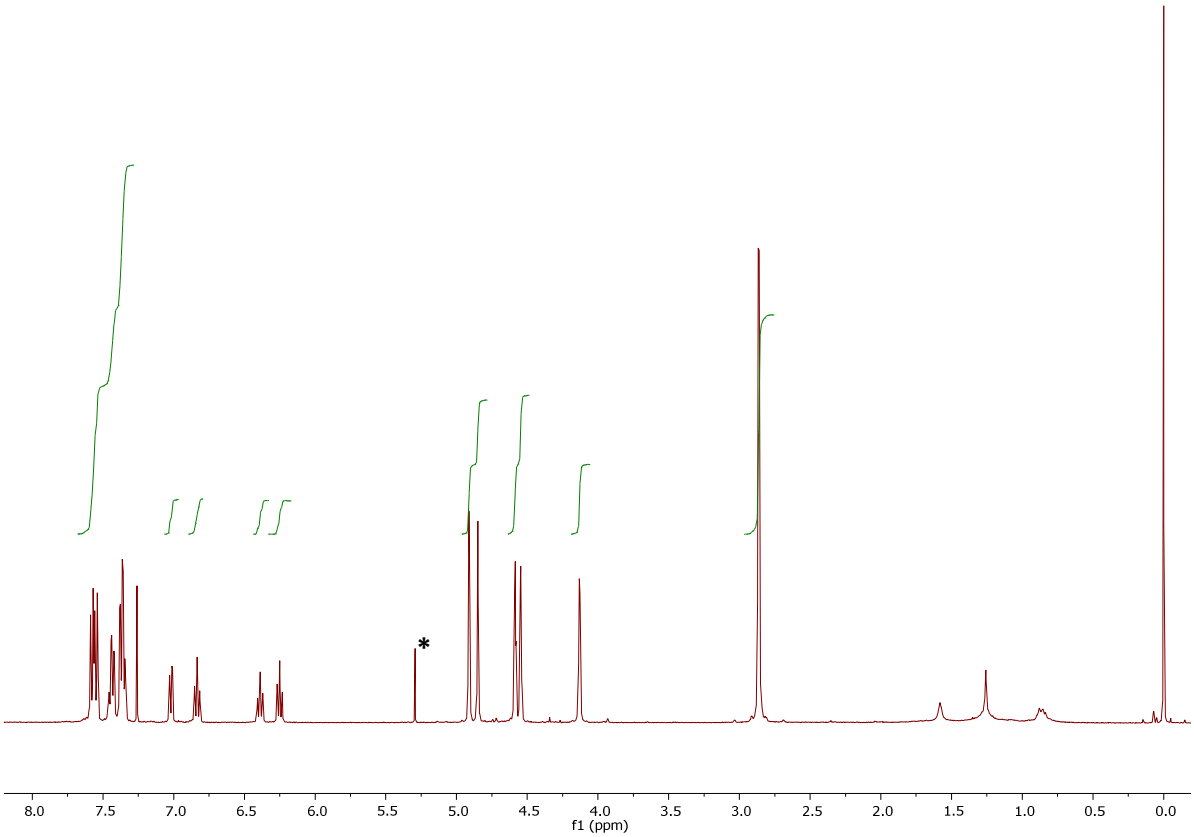

Figure S18. ^{1}H NMR (400 MHz, $CDCl_3$) spectrum of **8** (the signal due to residual CH_2Cl_2 is indicated by an asterisk).

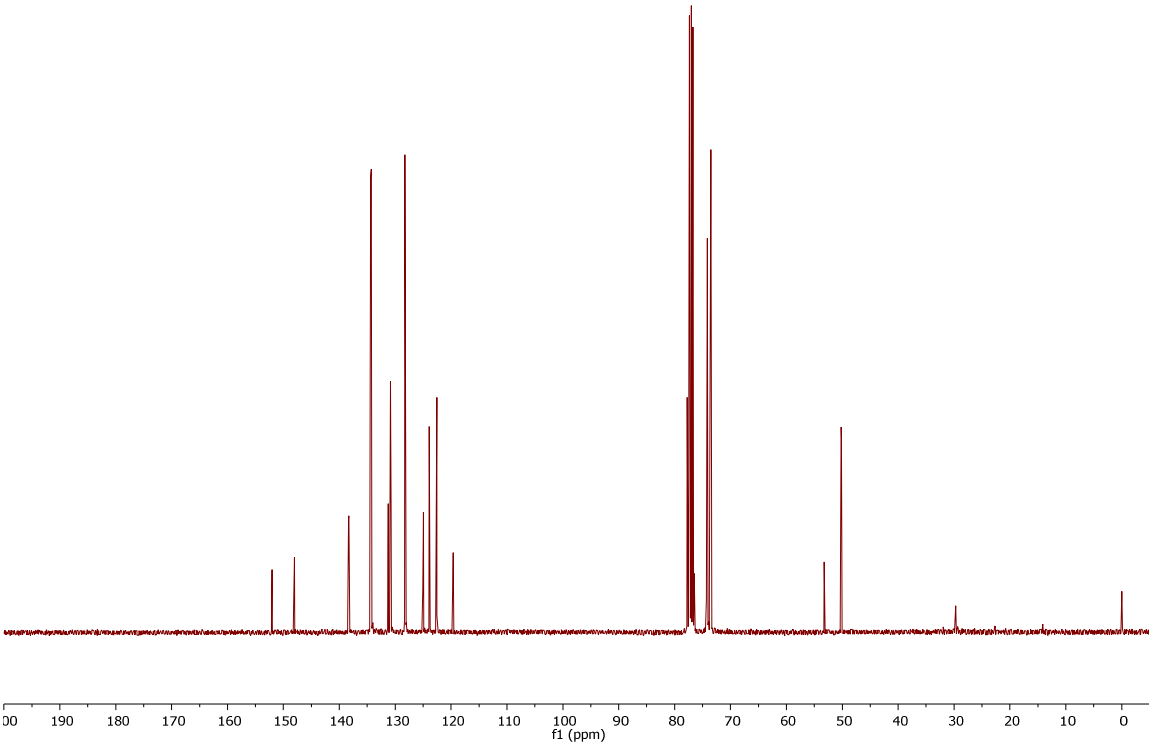

Figure S19. $^{13}C\{^{1}H\}$ NMR (101 MHz, $CDCl_3$) spectrum of **8**.

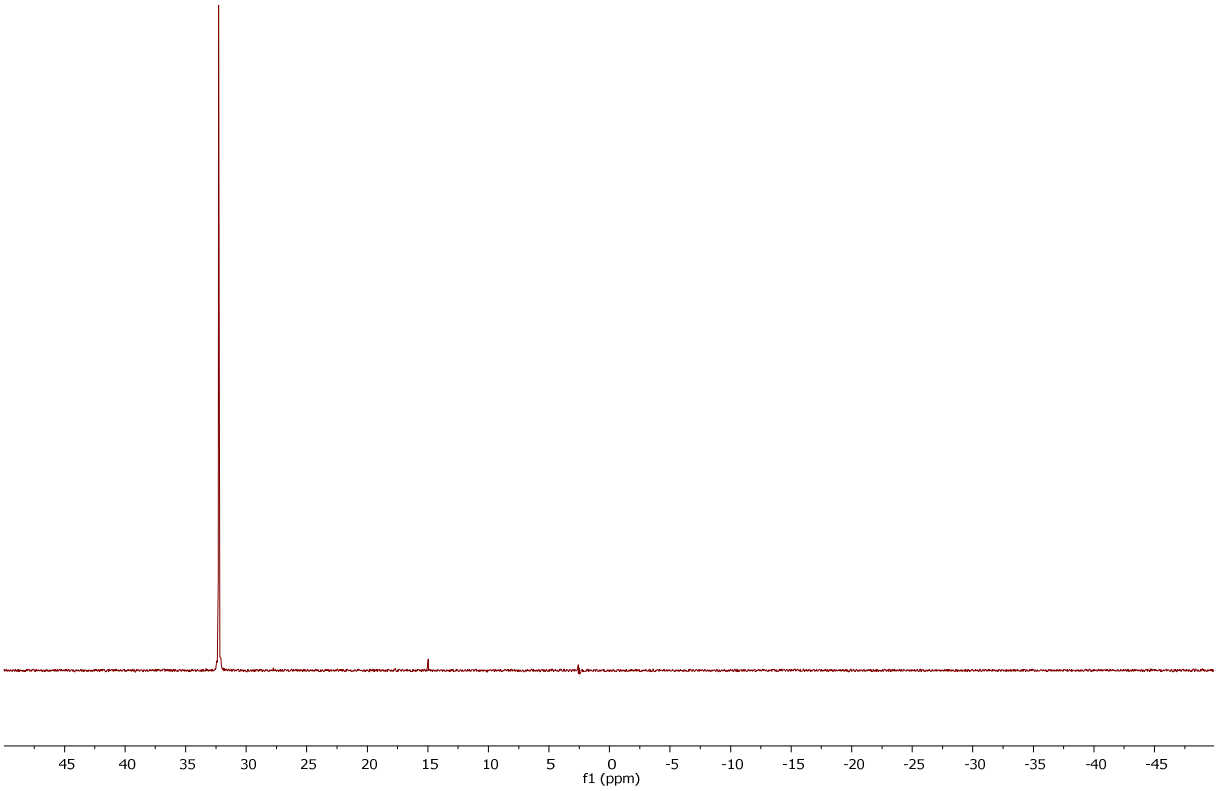

Figure S20. $^{31}P\{^{1}H]$ NMR (162 MHz, $CDCl_3$) spectrum of **8**.

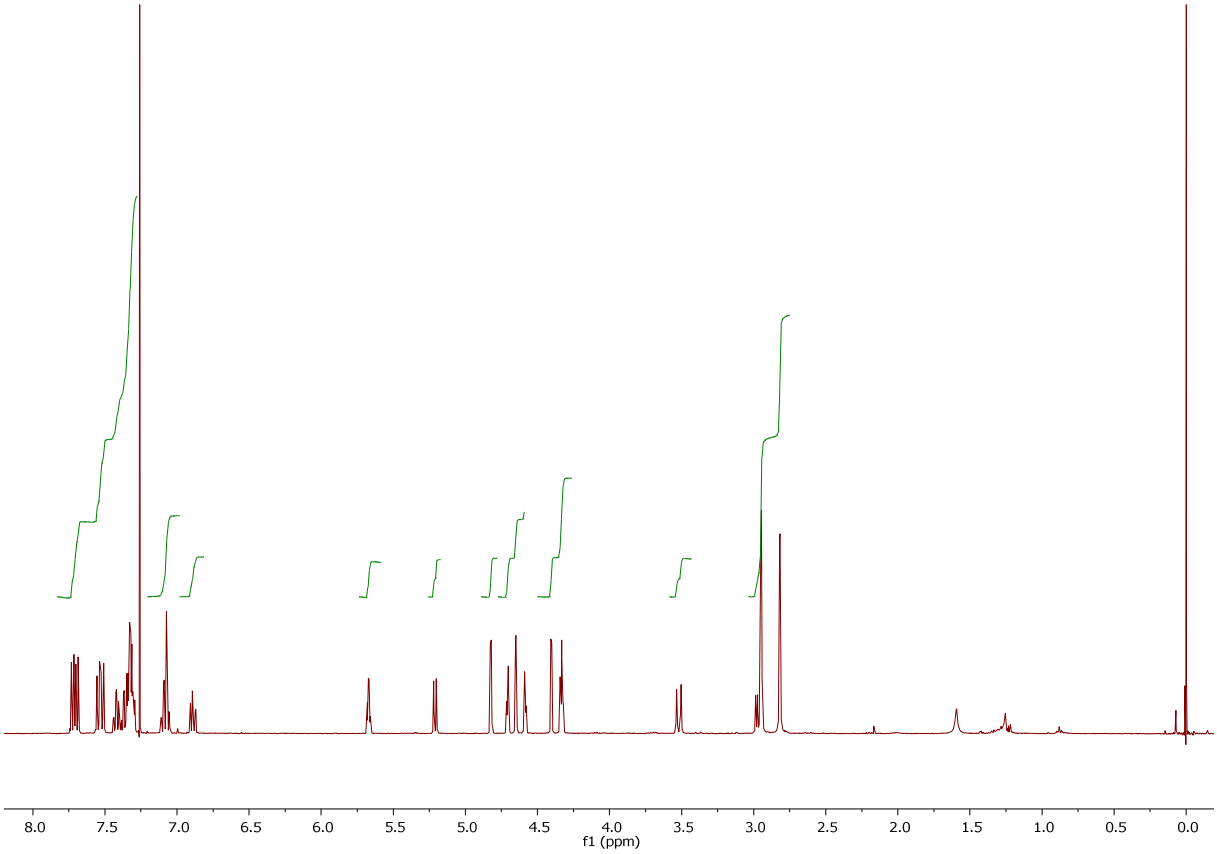

Figure S21. ^{1}H NMR (400 MHz, $CDCl_3$) spectrum of **10**.

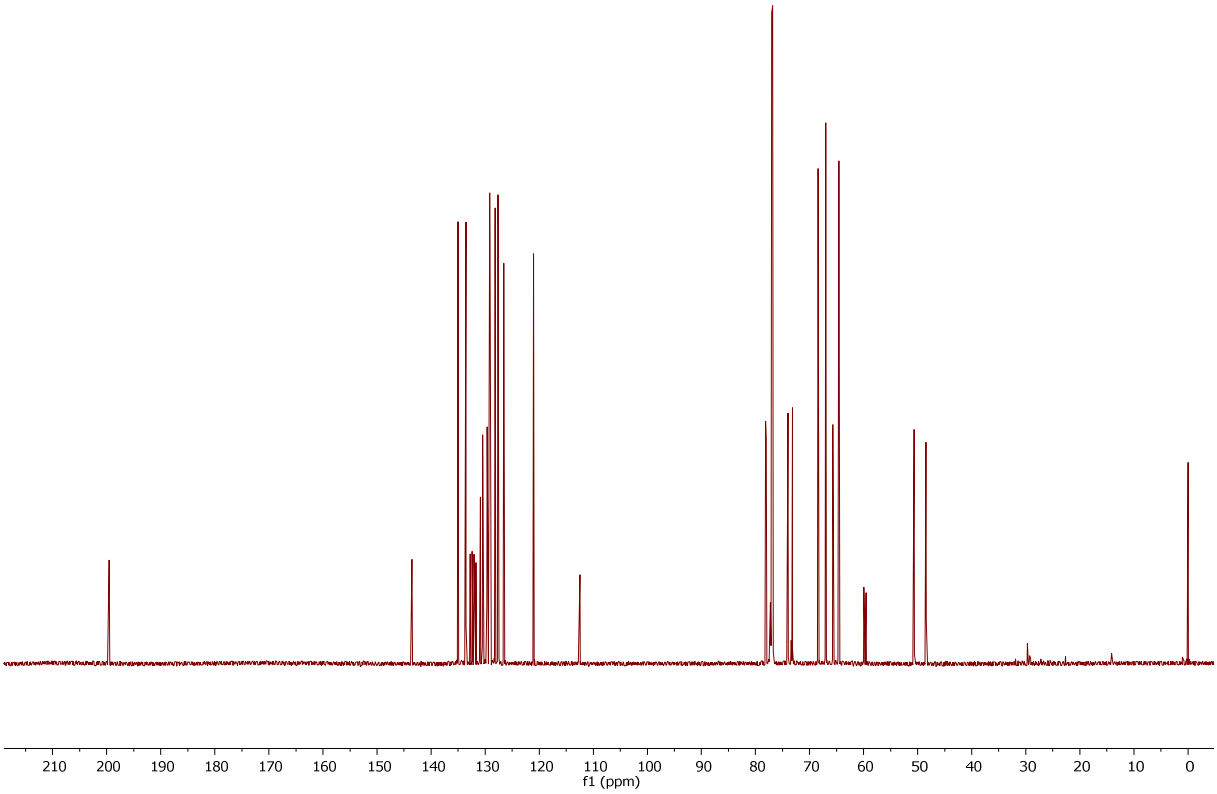

Figure S22. $^{13}C\{^{1}H\}$ NMR (151 MHz, $CDCl_3$) spectrum of **10**.

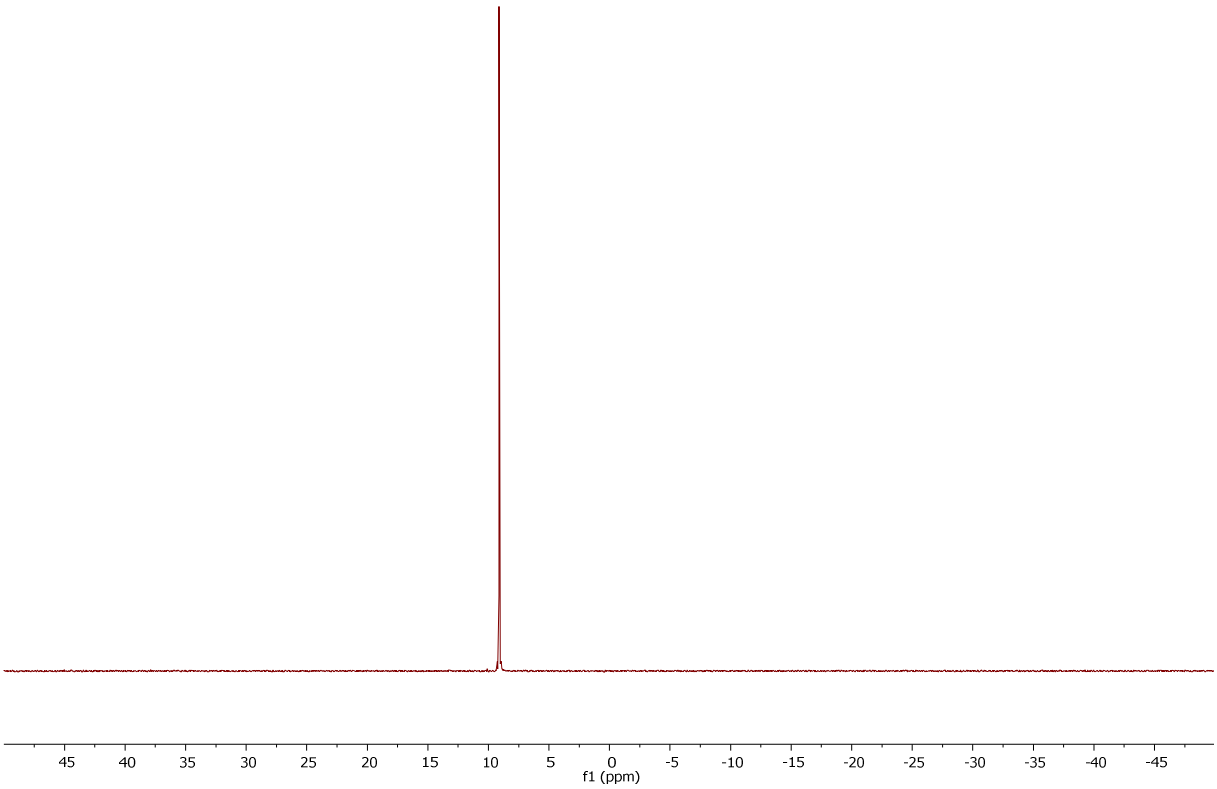

Figure S23. $^{31}P\{^{1}H\}$ NMR (162 MHz, $CDCl_3$) spectrum of **10**.

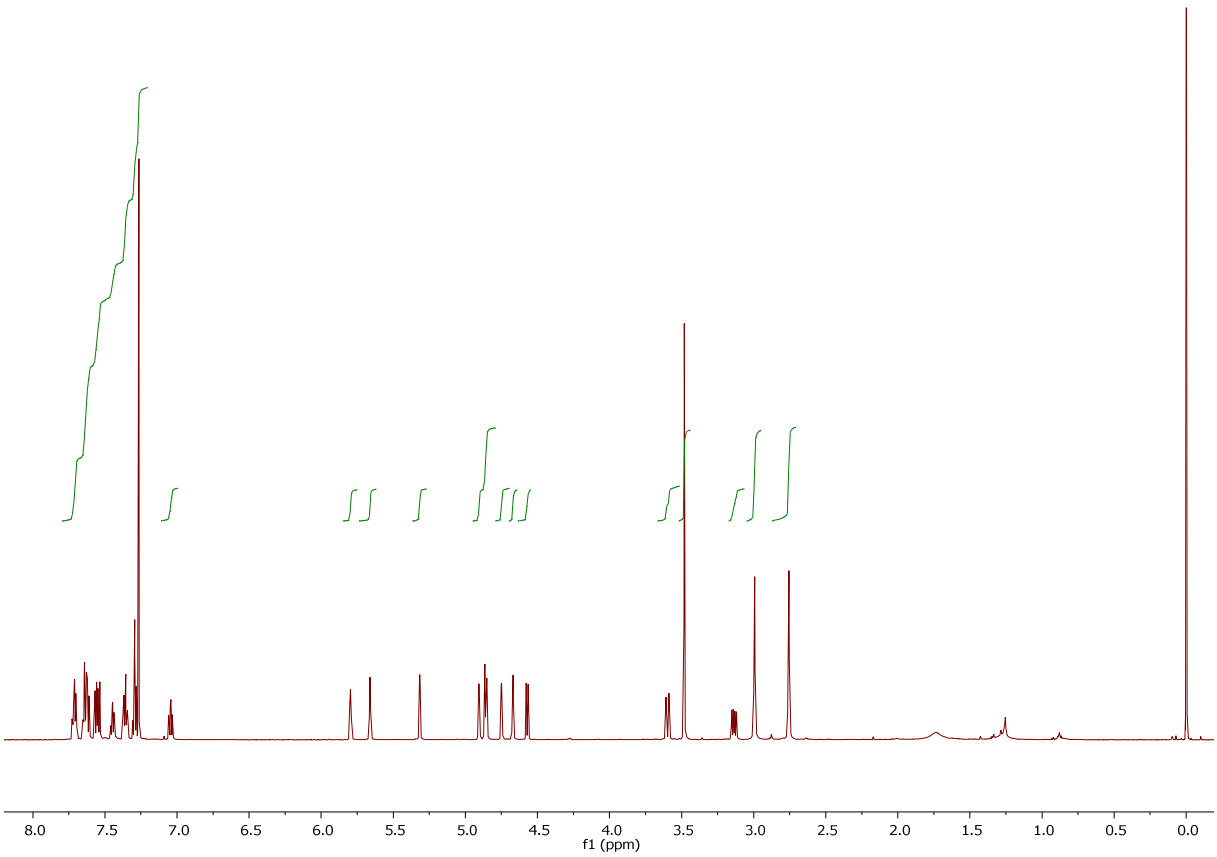

Figure S24. ^{1}H NMR (600 MHz, $CDCl_3$) spectrum of **11**.

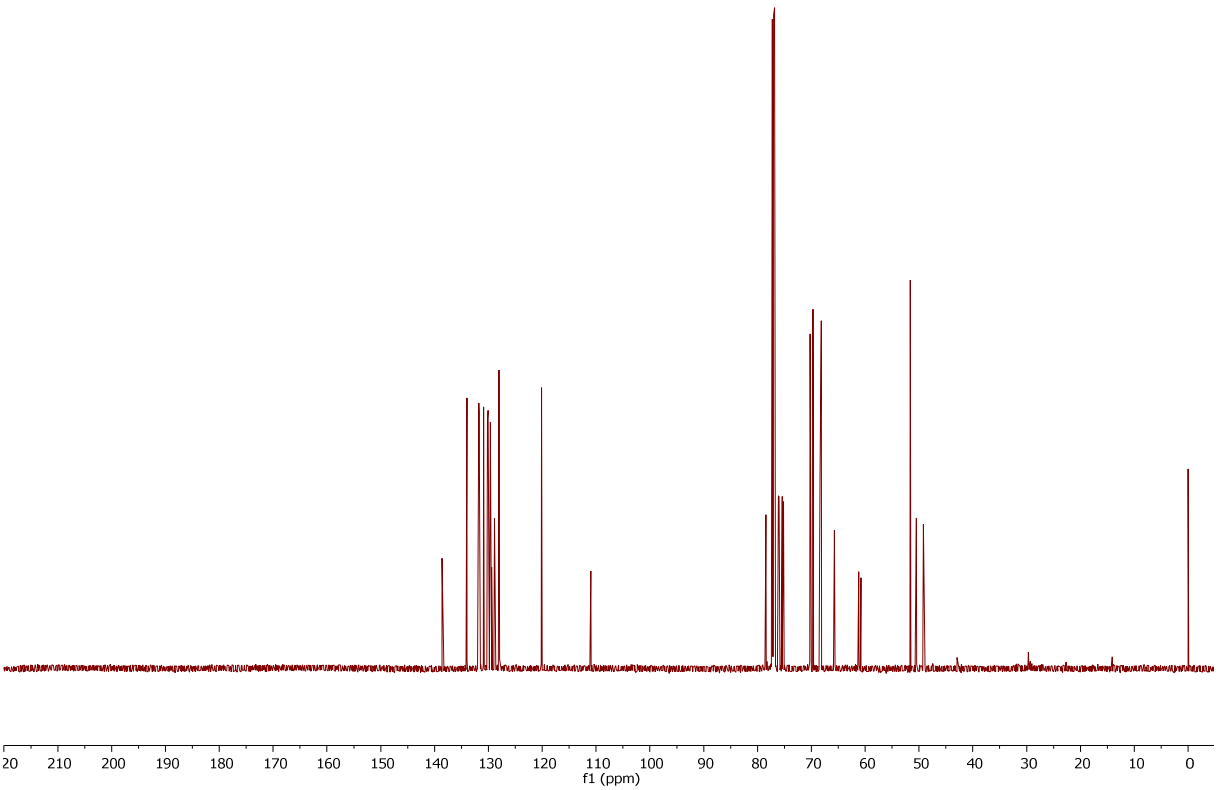

Figure S25. $^{13}C\{^{1}H\}$ NMR (151 MHz, $CDCl_3$) spectrum of **11**.

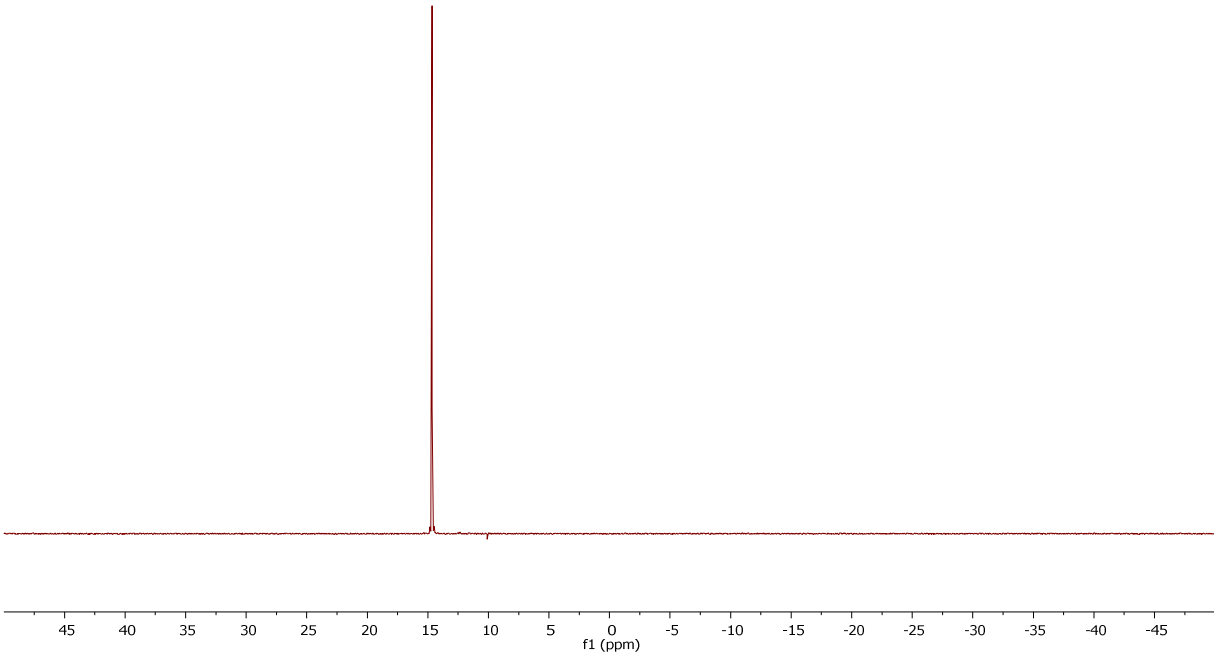

Figure S26. $^{31}P\{^{1}H]$ NMR (162 MHz, $CDCl_3$) spectrum of **11**.

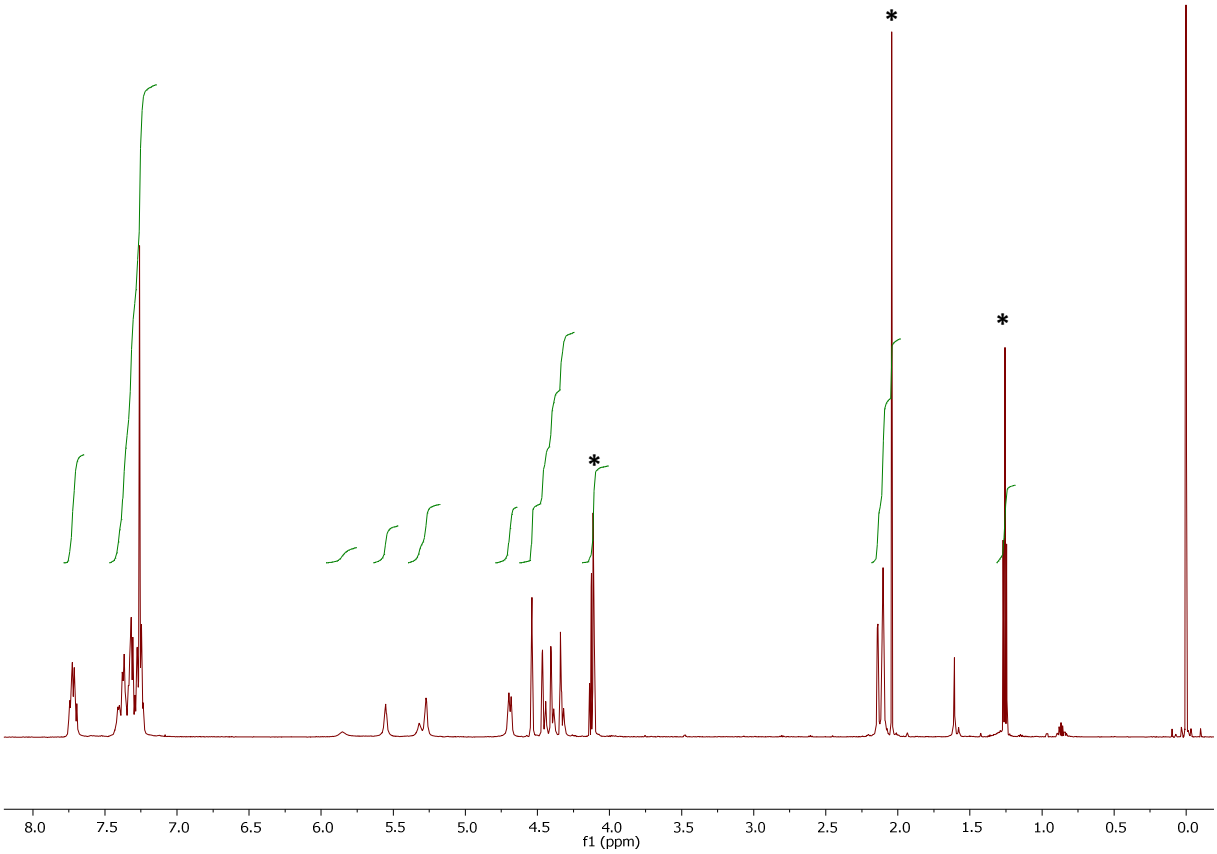

Figure S27. ^{1}H NMR (600 MHz, $CDCl_3$) spectrum of **12** (signals due to residual AcOEt are indicated by an asterisk).

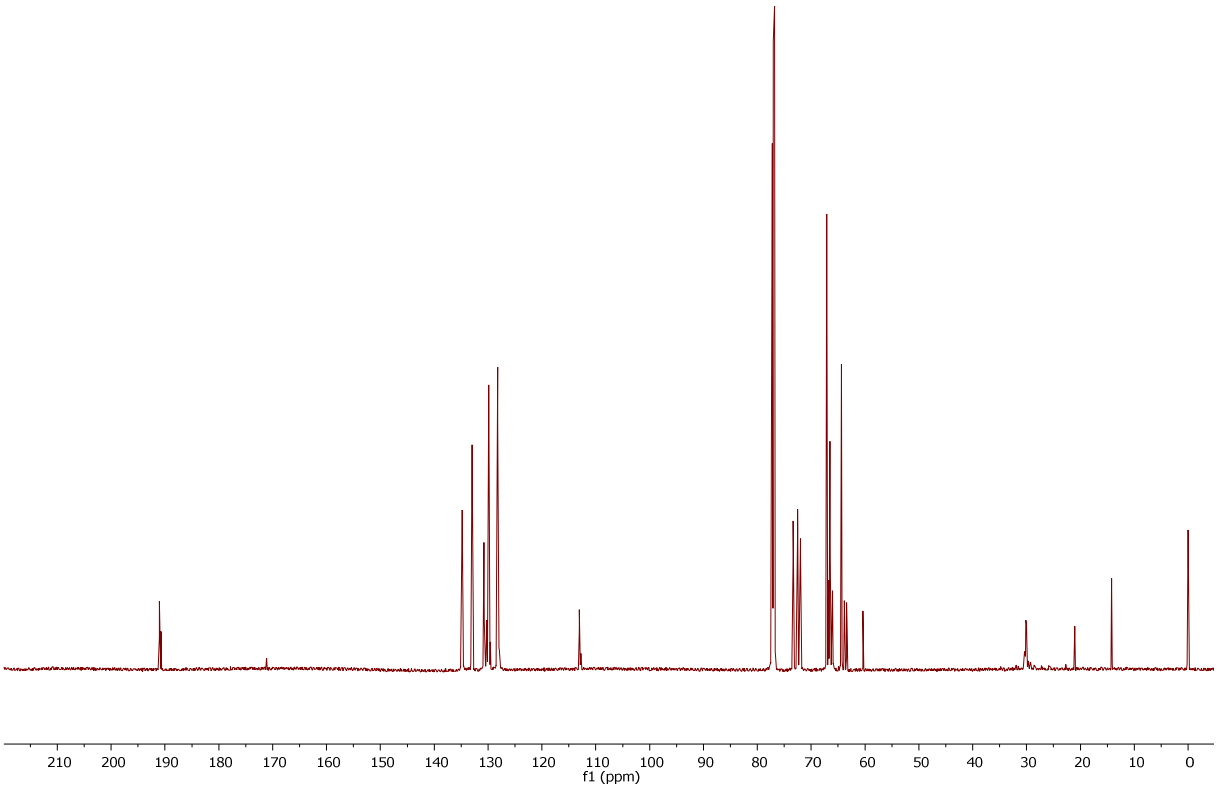

Figure S28. $^{13}C\{^{1}H\}$ NMR (151 MHz, $CDCl_3$) spectrum of **12**.

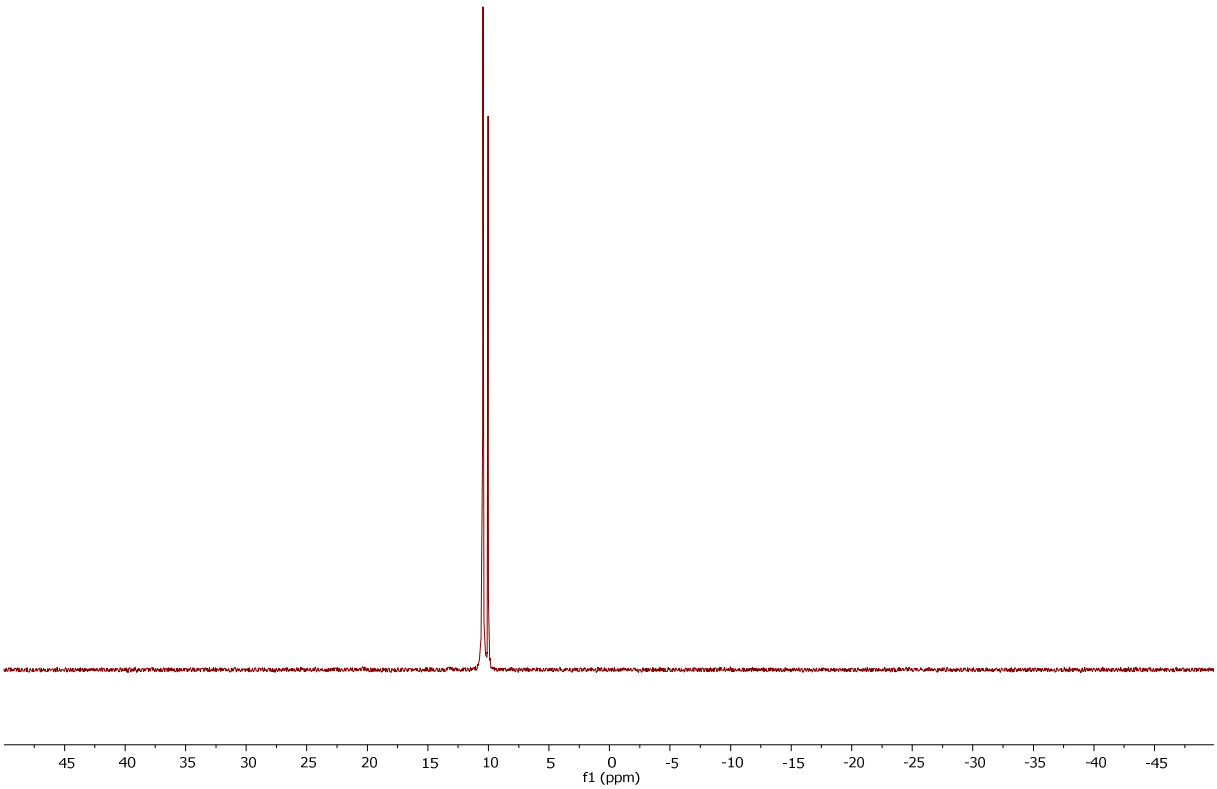

Figure S29. $^{31}P\{^{1}H\}$ NMR (162 MHz, $CDCl_3$) spectrum of **12**.

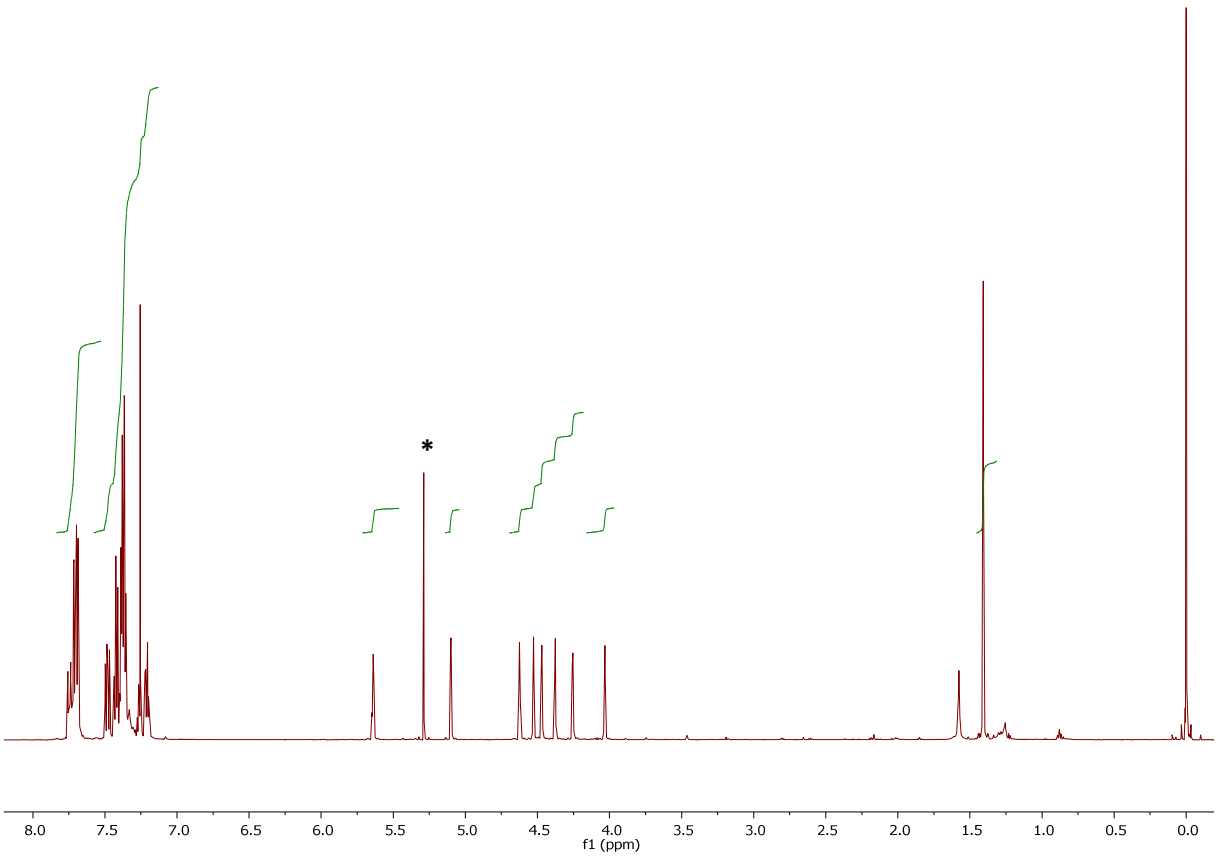

Figure S30. ^{1}H NMR (600 MHz, $CDCl_3$) spectrum of **13** (the signal due to residual CH_2Cl_2 is indicated by an asterisk).

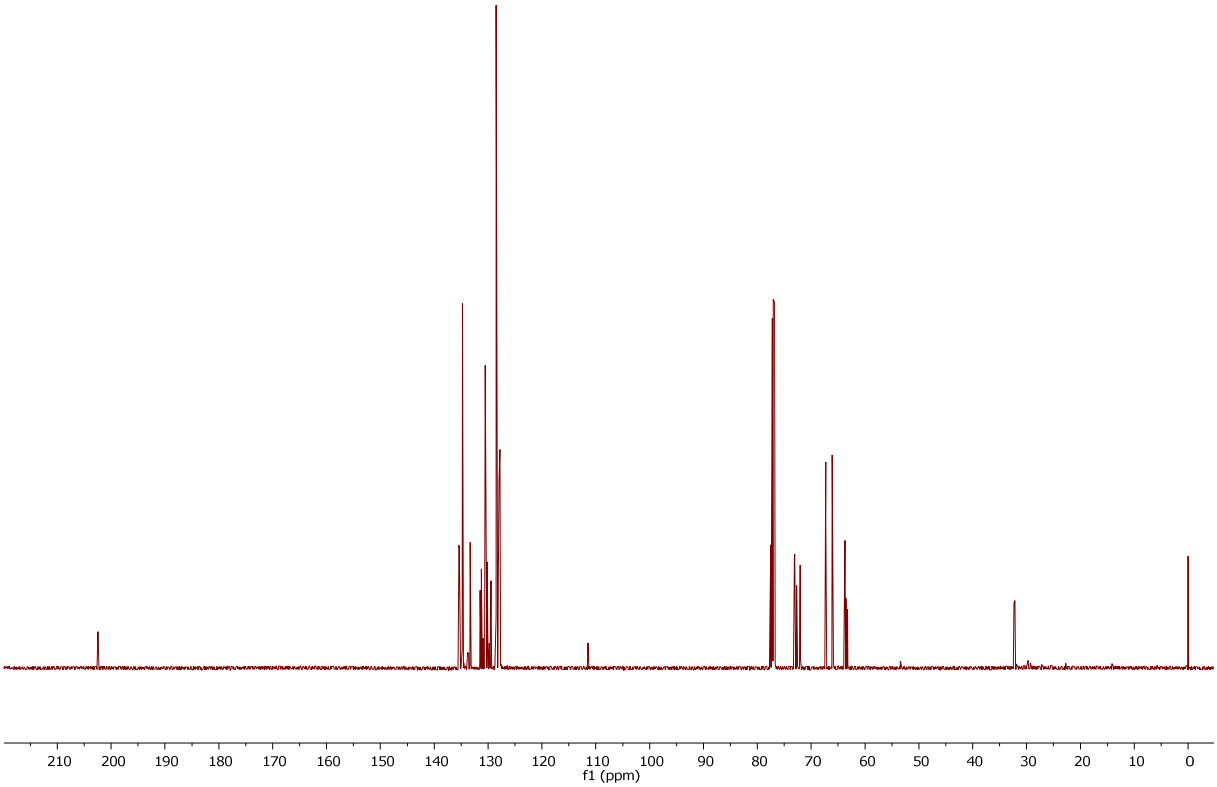

Figure S31. $^{13}C\{^{1}H\}$ NMR (151 MHz, $CDCl_3$) spectrum of **13**.

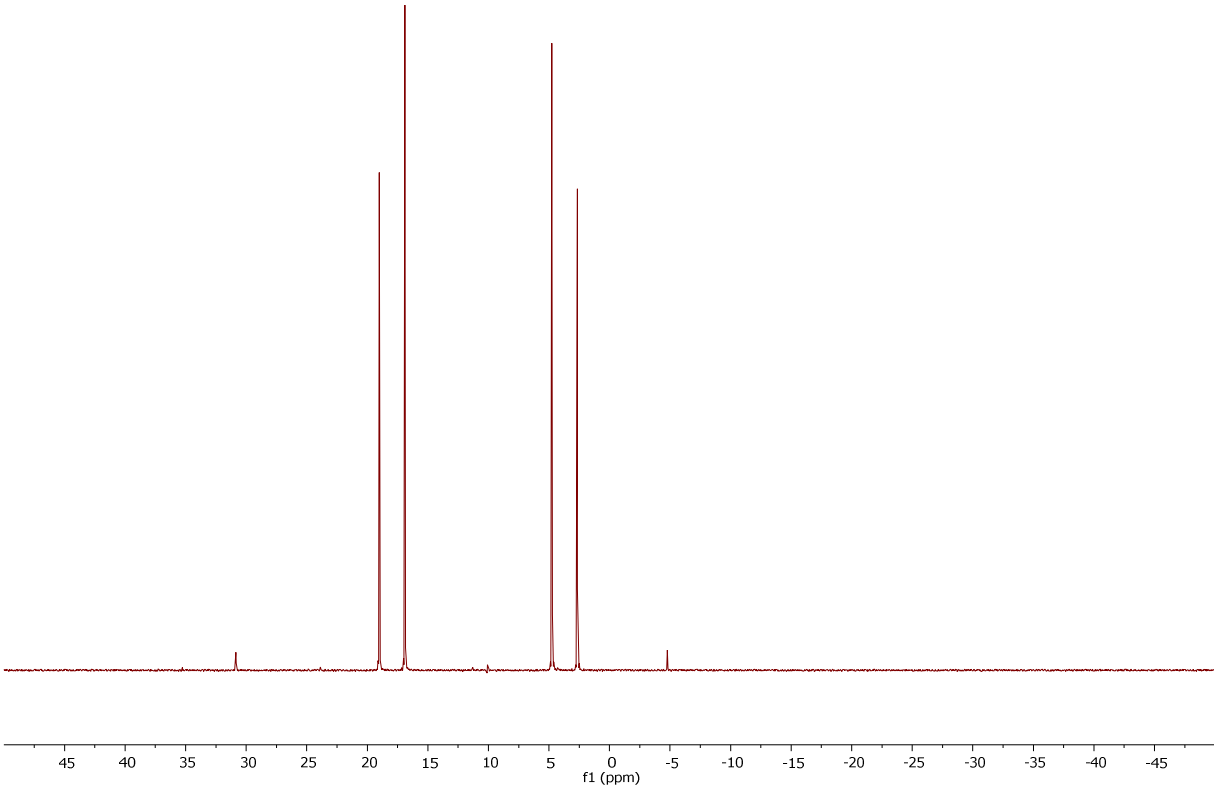

Figure S32. $^{31}P\{^{1}H]$ NMR (162 MHz, $CDCl_3$) spectrum of **13**. The minor signals at $\delta_P \approx -5$ and 32 ppm are due to traces of triphenylphosphine and phosphine oxide of **2**, respectively.

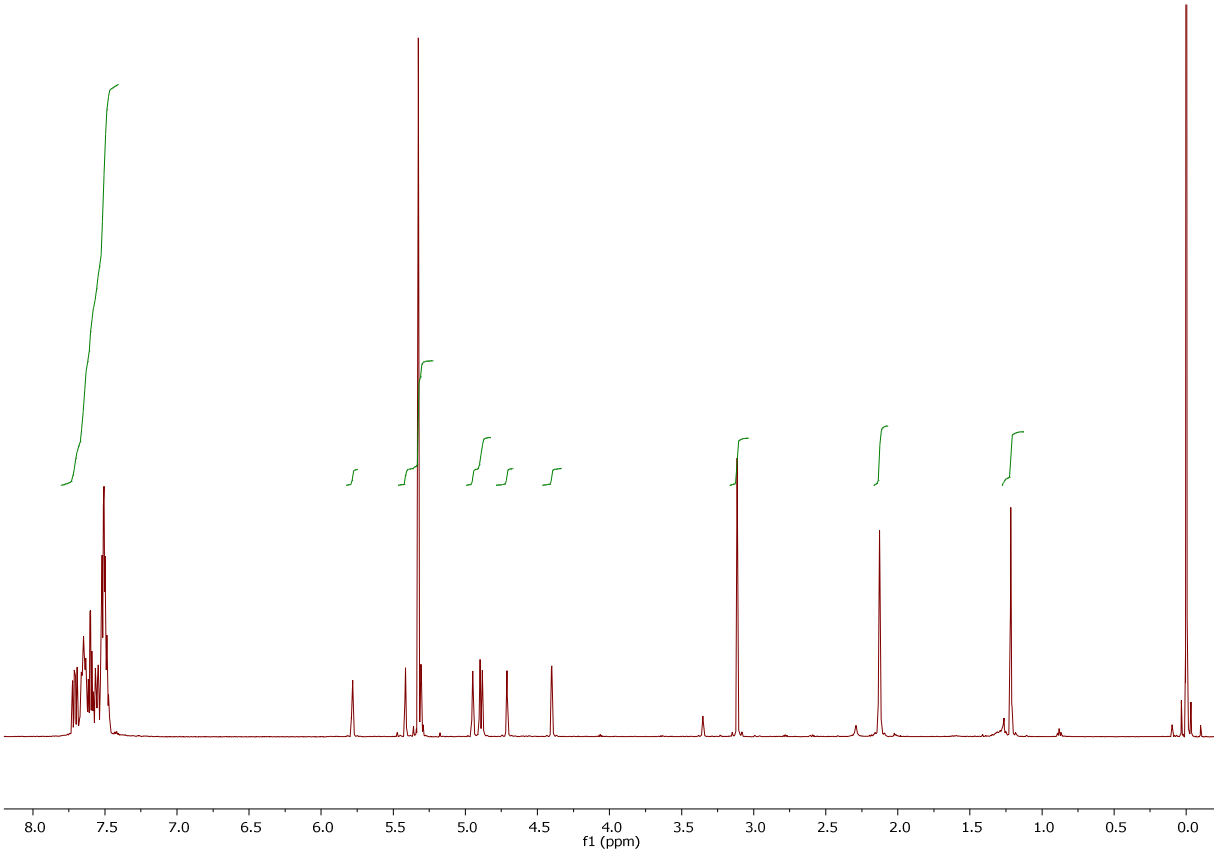

Figure S33. ^{1}H NMR (600 MHz, CD_2Cl_2/CD_3OD) spectrum of **14**.

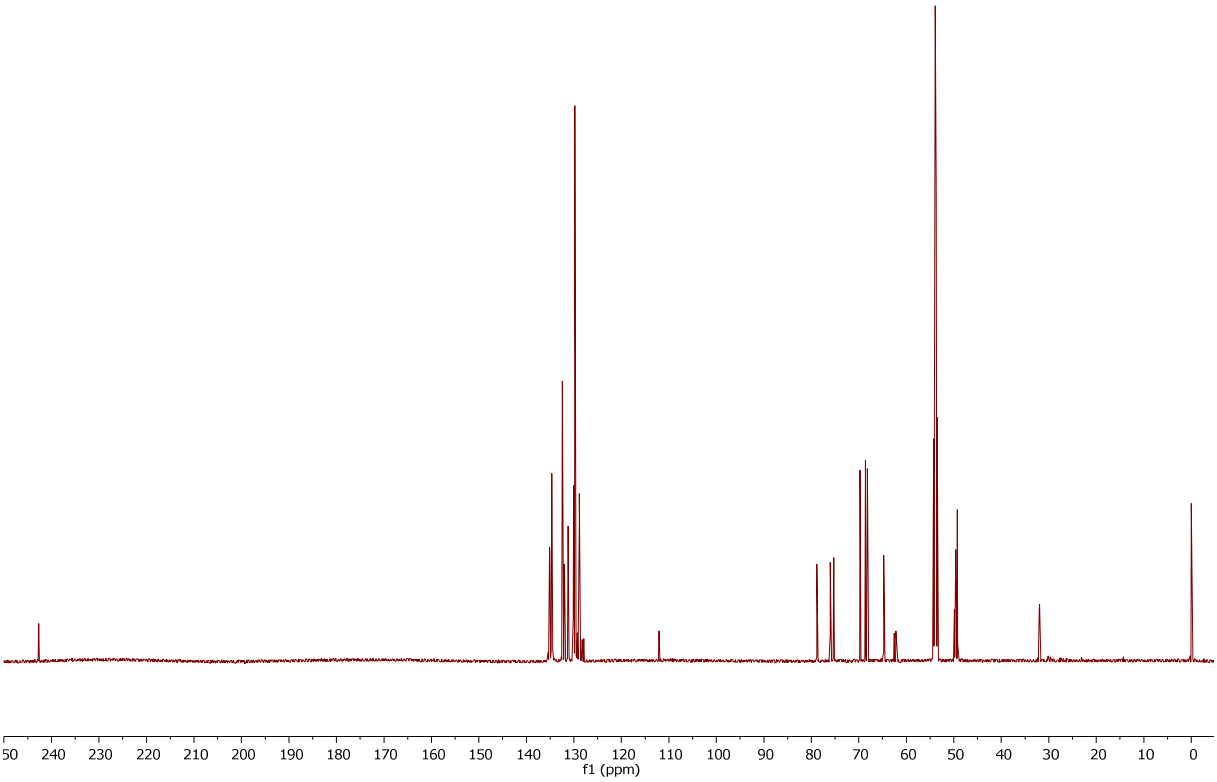

Figure S34. $^{13}C\{^{1}H\}$ NMR (151 MHz, CD_2Cl_2/CD_3OD) spectrum of **14**.

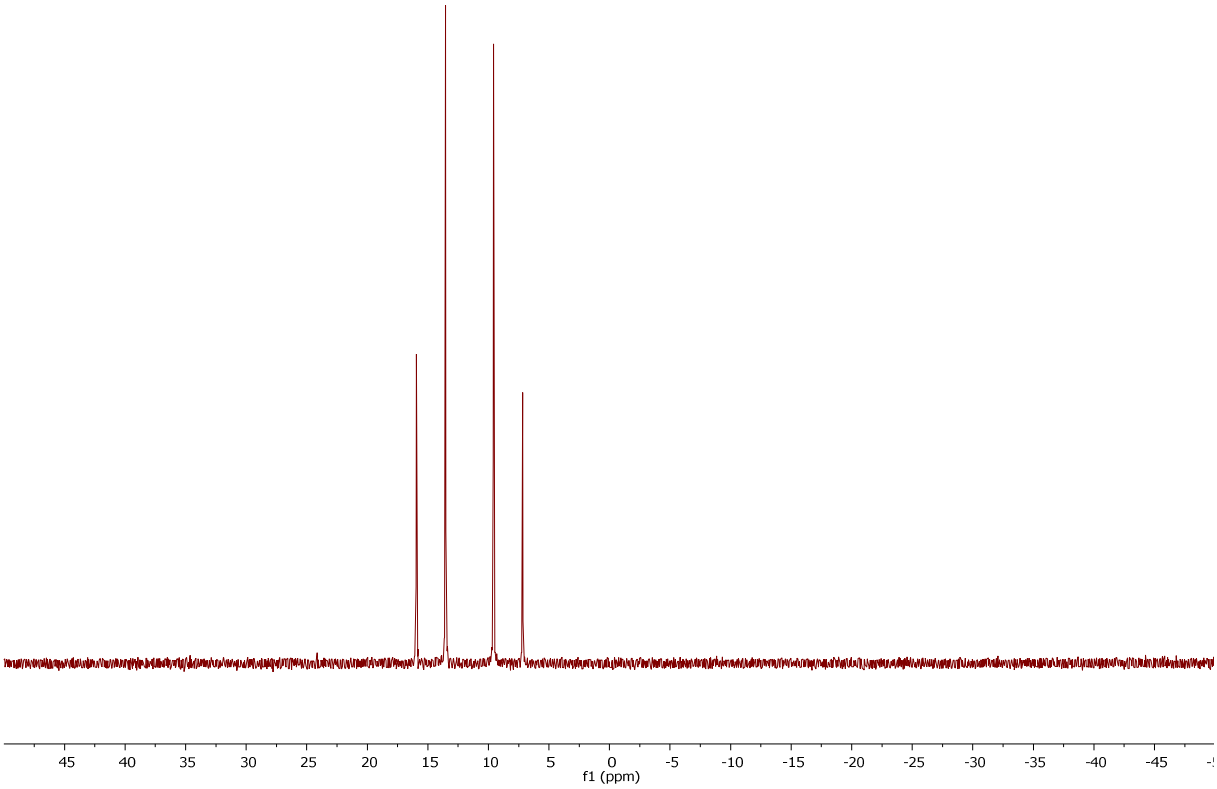

Figure S35. $^{31}P\{^{1}H\}$ NMR (162 MHz, CD_2Cl_2/CD_3OD) spectrum of **14**.

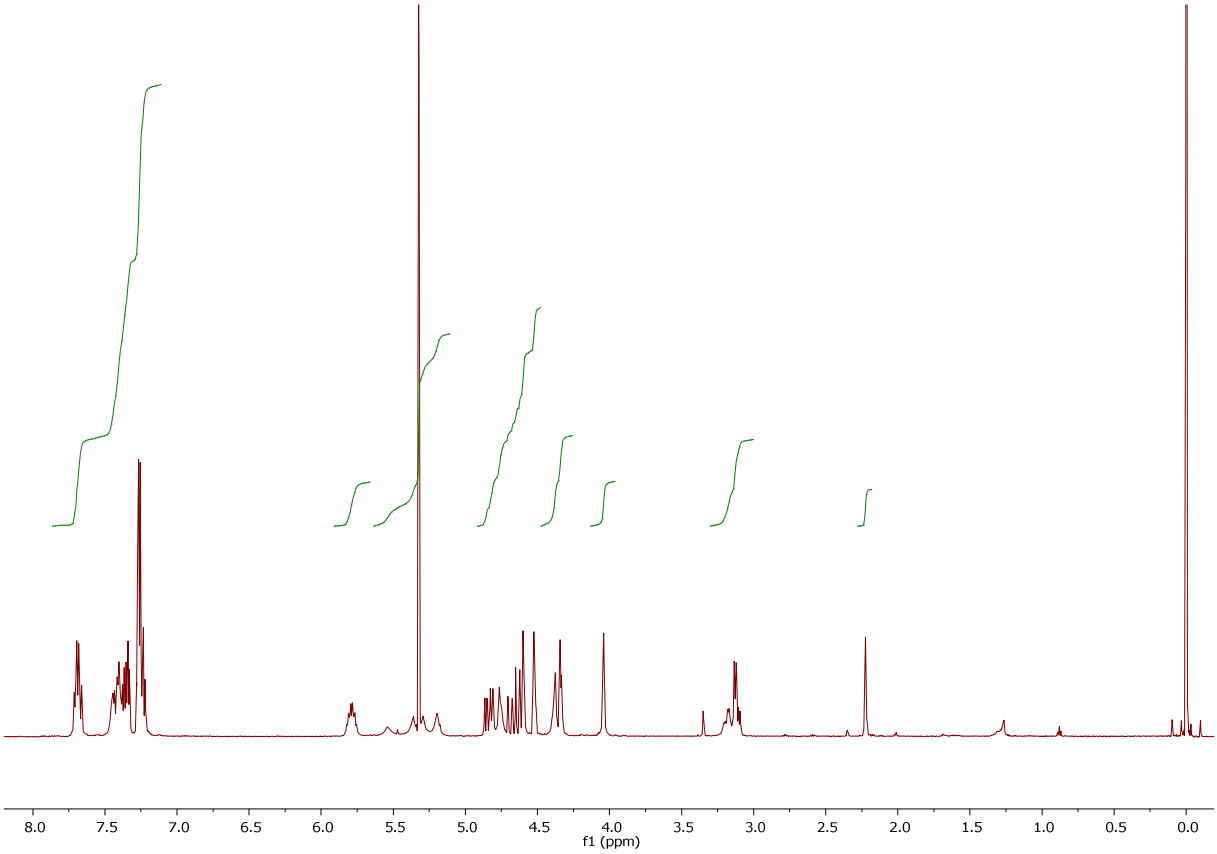

Figure S36. ^{1}H NMR (600 MHz, CD_2Cl_2/CD_3OD) spectrum of **15**.

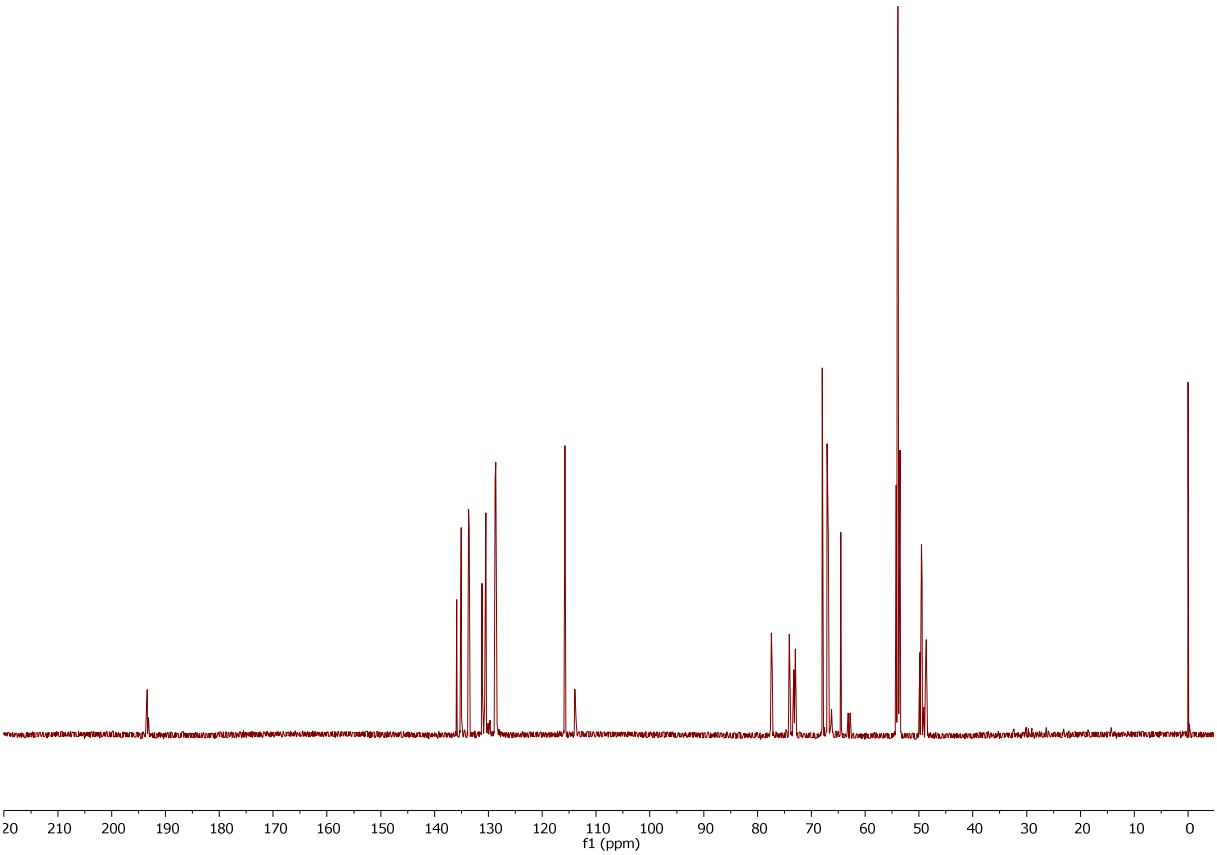

Figure S37. $^{13}C\{^{1}H\}$ NMR (151 MHz, CD_2Cl_2/CD_3OD) spectrum of **15**.

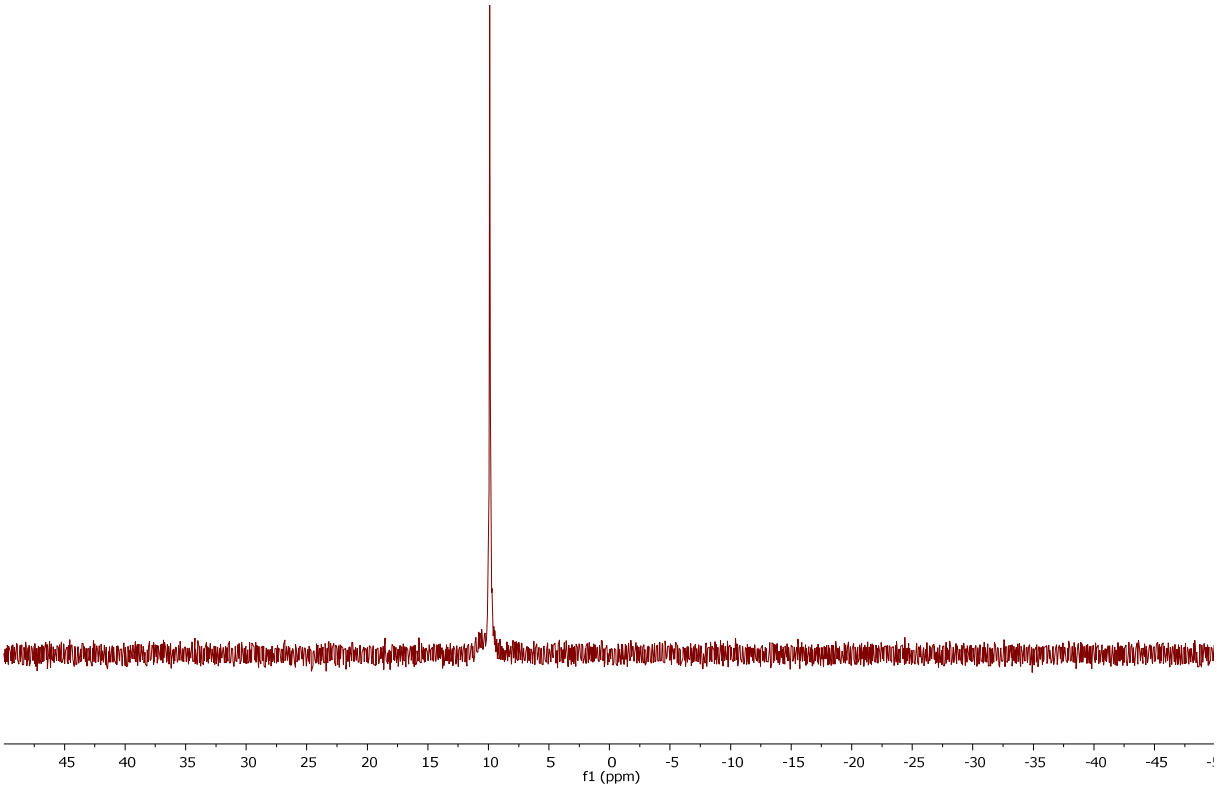

Figure S38. $^{31}P\{^{1}H]$ NMR (162 MHz, CD_2Cl_2/CD_3OD) spectrum of **15**.

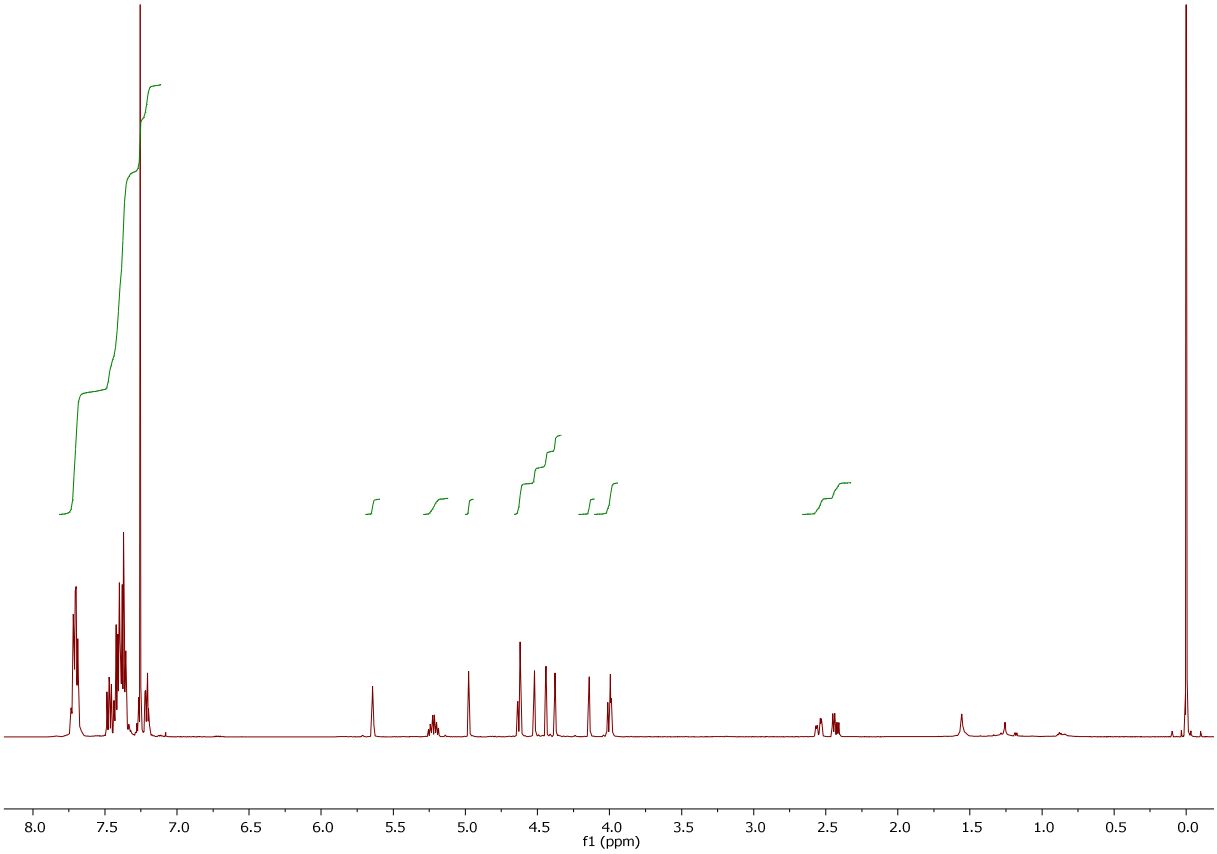

Figure S39. ^{1}H NMR (600 MHz, $CDCl_3$) spectrum of **16**.

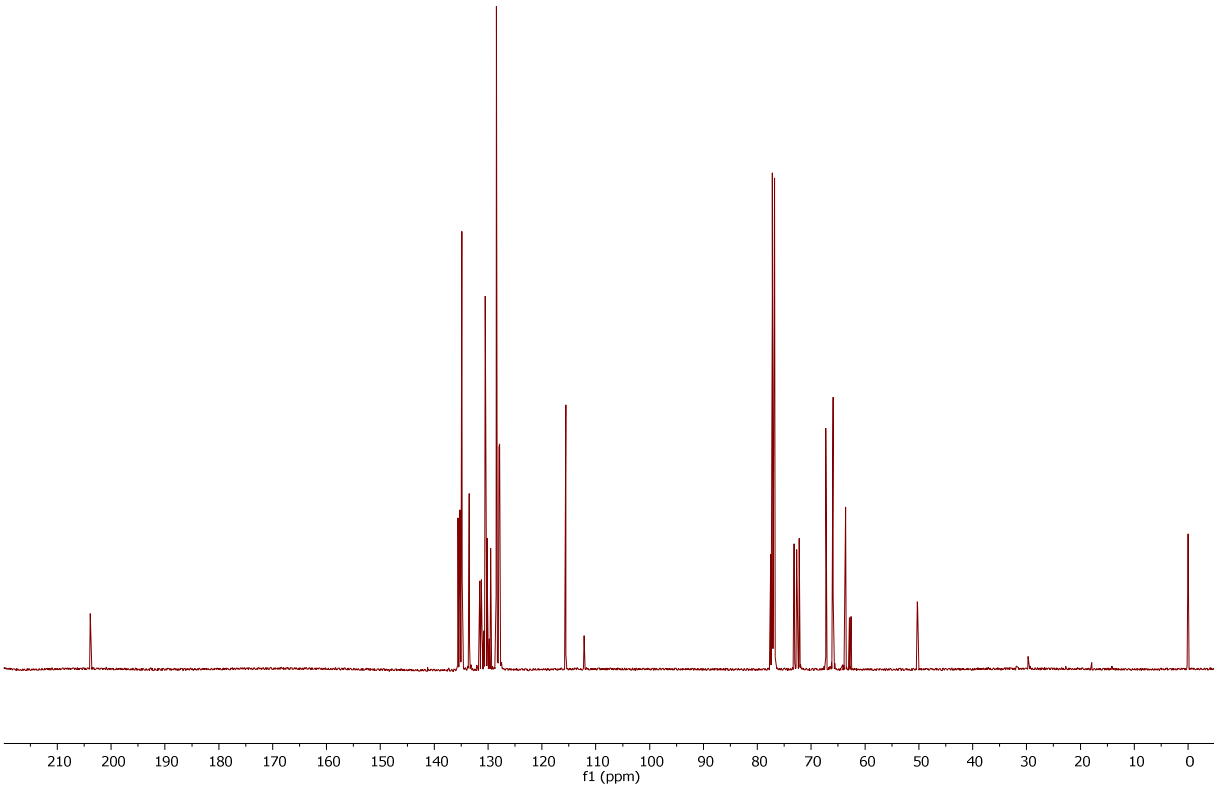

Figure S40. $^{13}C\{^{1}H\}$ NMR (151 MHz, $CDCl_3$) spectrum of **16**.

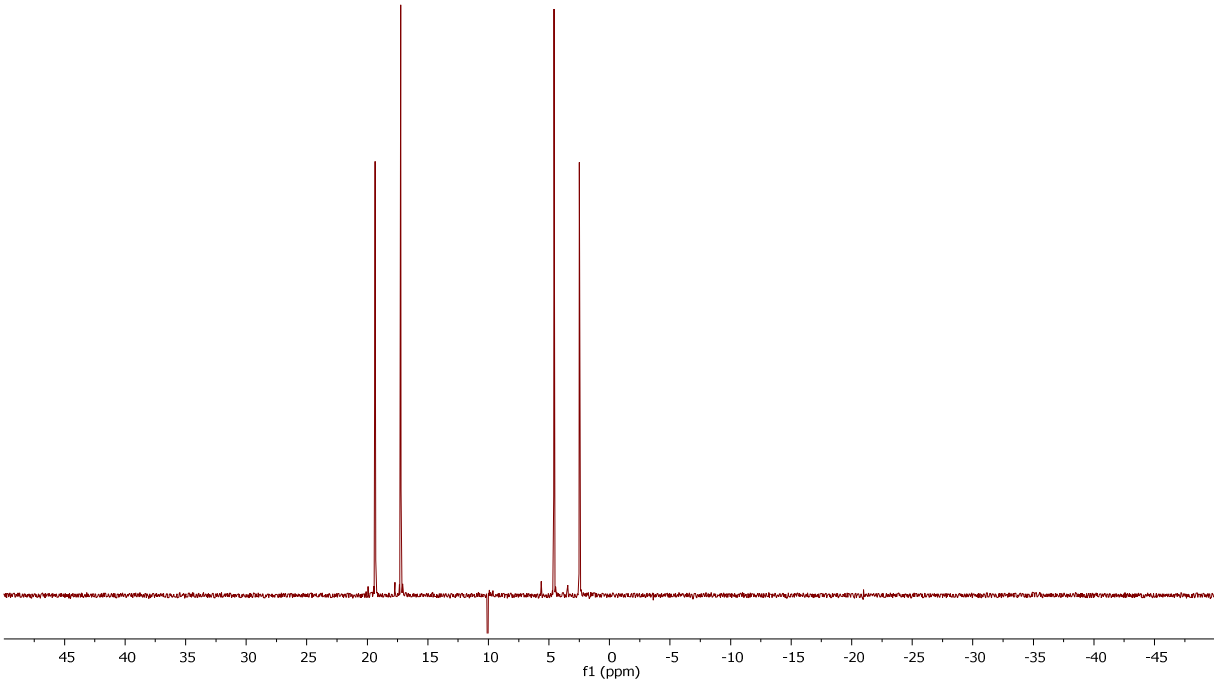

Figure S41. $^{31}P\{^{1}H]$ NMR (162 MHz, $CDCl_3$) spectrum of **16**.

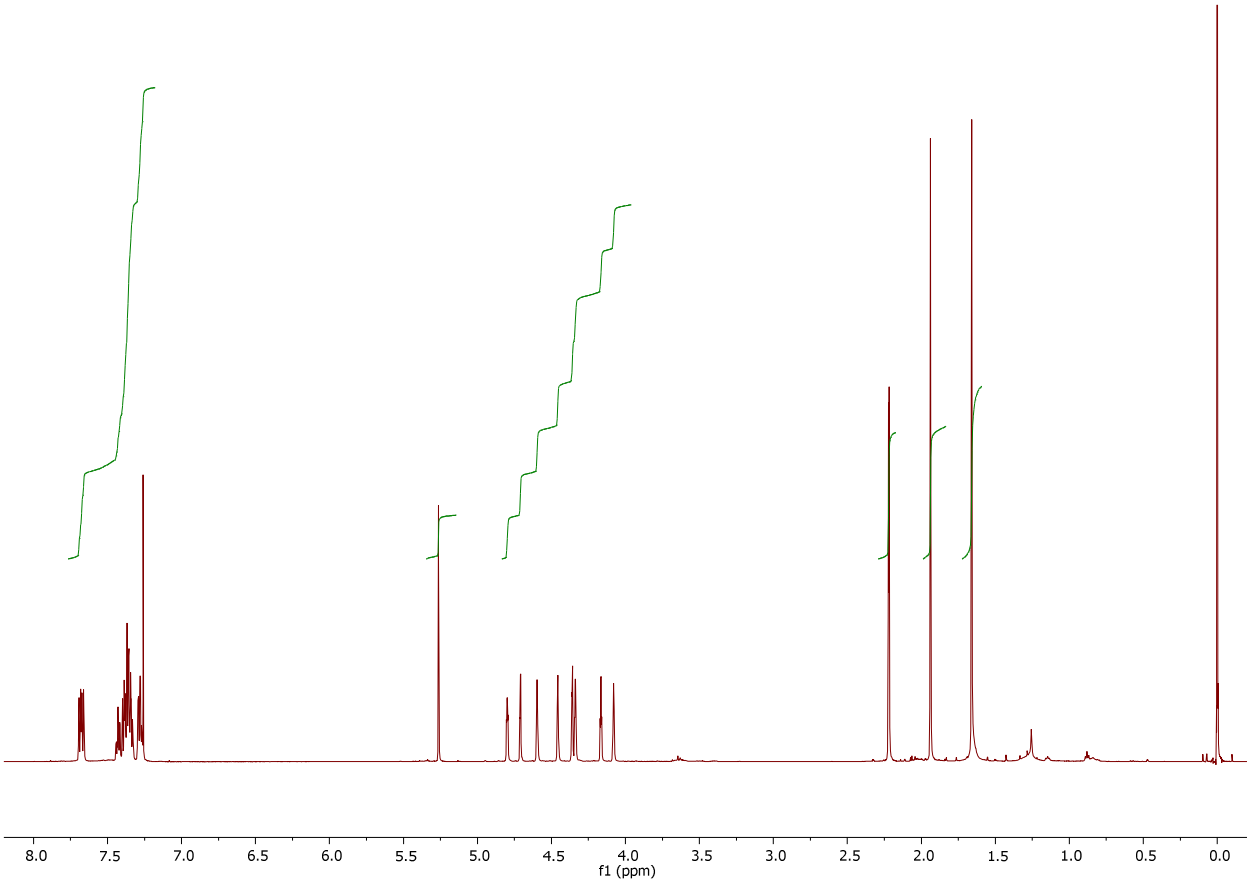

Figure S42. ^{1}H NMR (600 MHz, $CDCl_3$) spectrum of **17**.

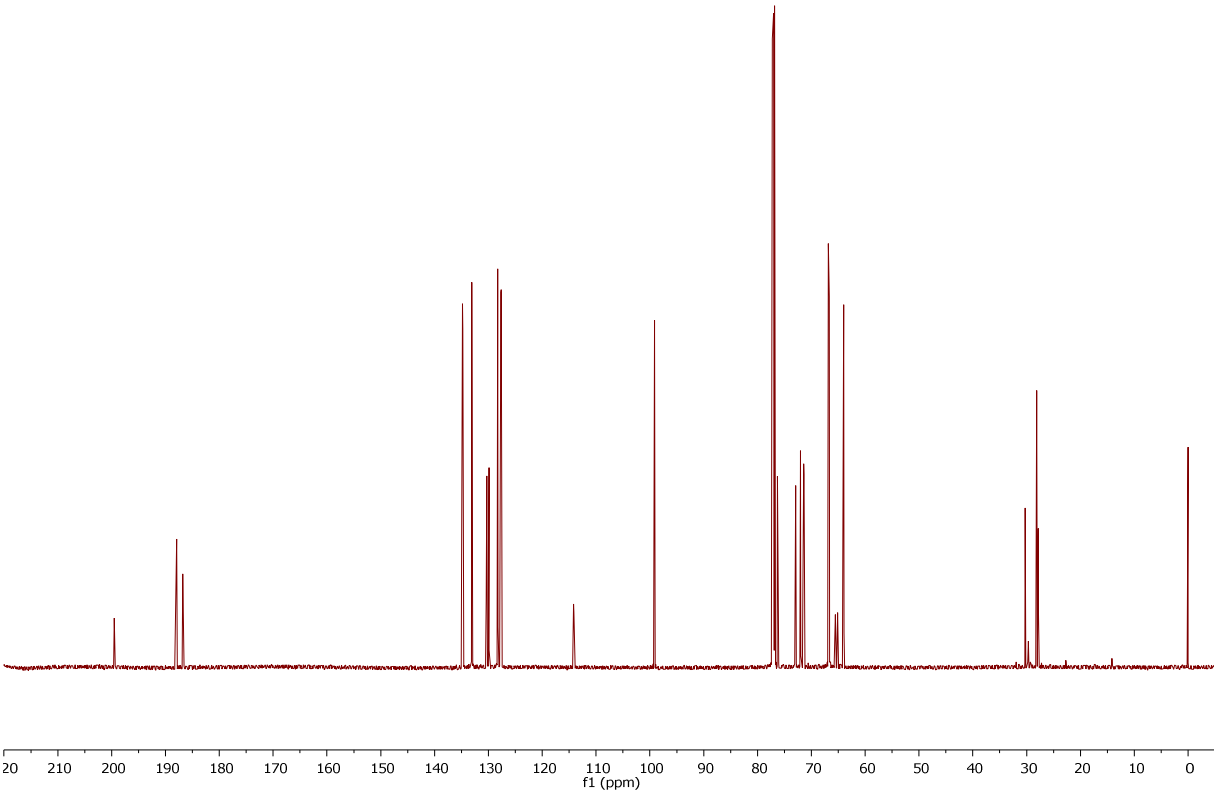

Figure S43. $^{13}C\{^{1}H\}$ NMR (151 MHz, $CDCl_3$) spectrum of **17**.

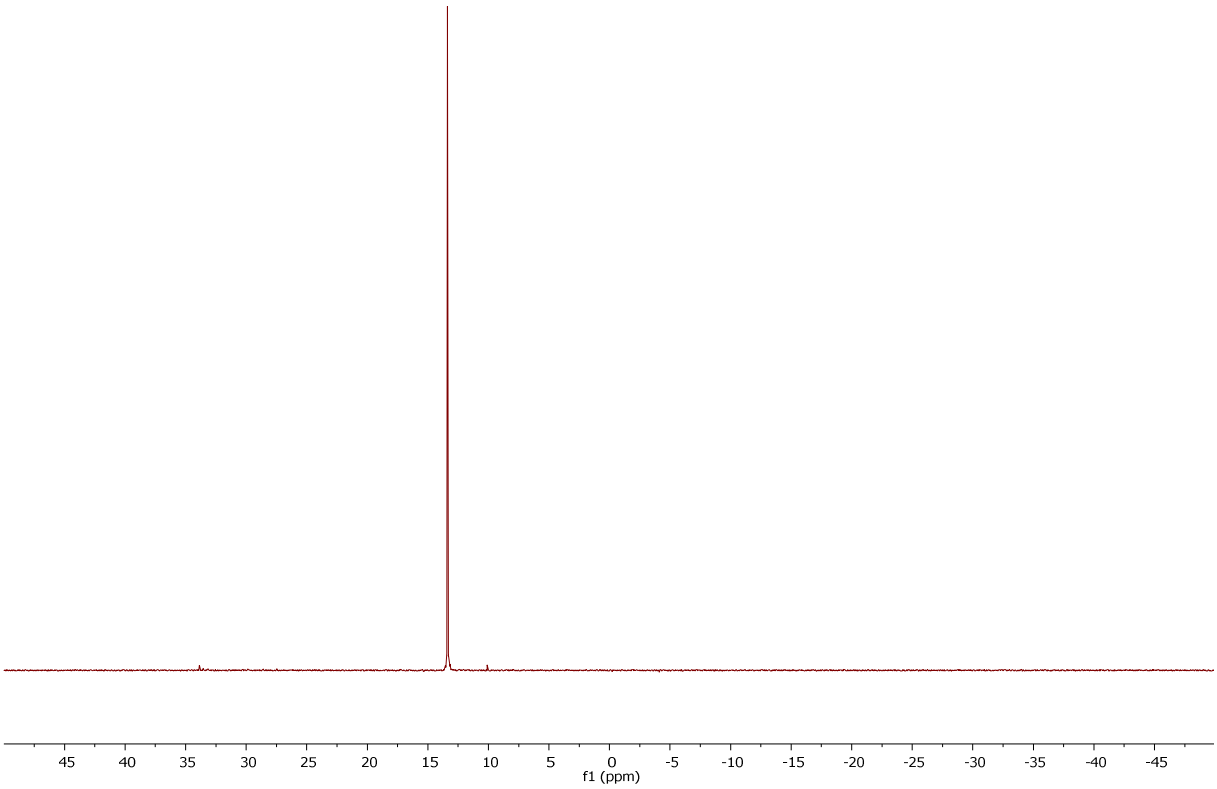

Figure S44. $^{31}P\{^{1}H]$ NMR (162 MHz, $CDCl_3$) spectrum of **17**.

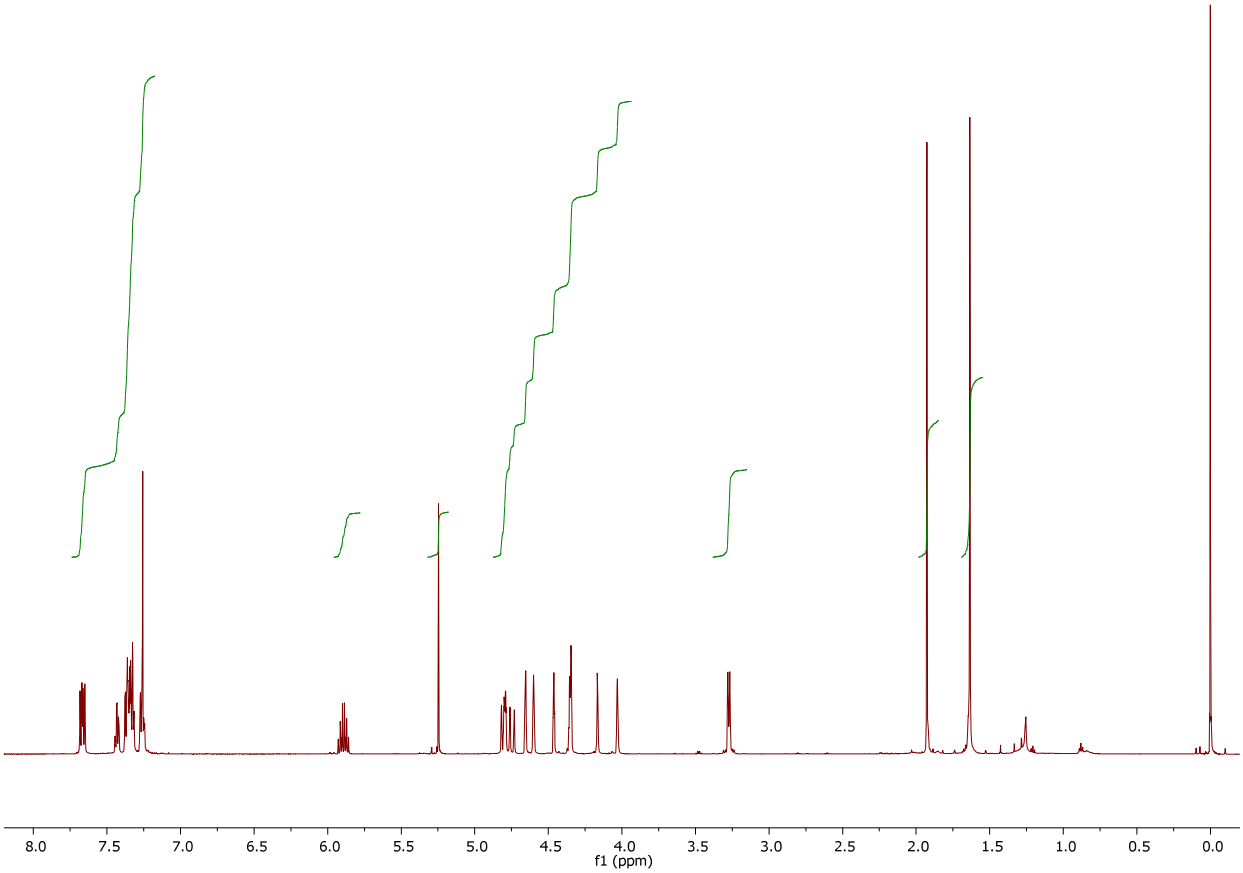

Figure S45. ^{1}H NMR (600 MHz, $CDCl_3$) spectrum of **18**

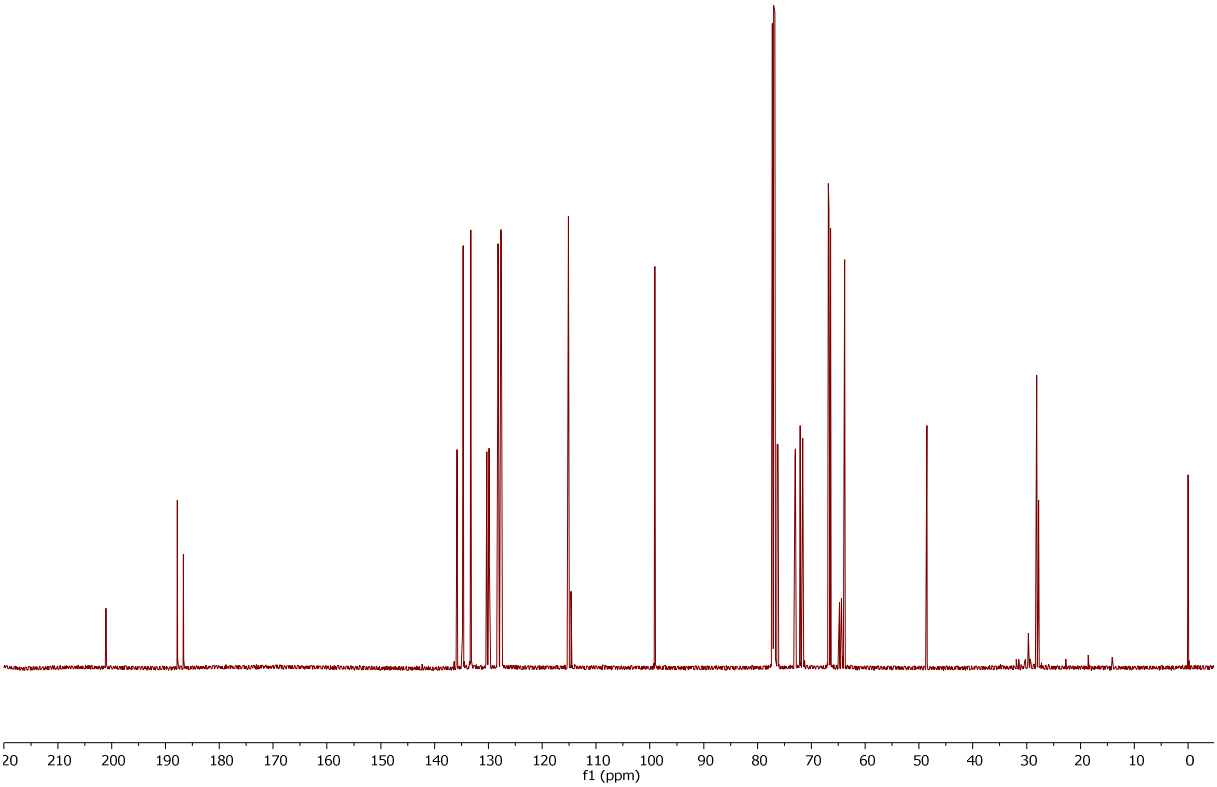

Figure S46. $^{13}C\{^{1}H\}$ NMR (151 MHz, $CDCl_3$) spectrum of **18**.

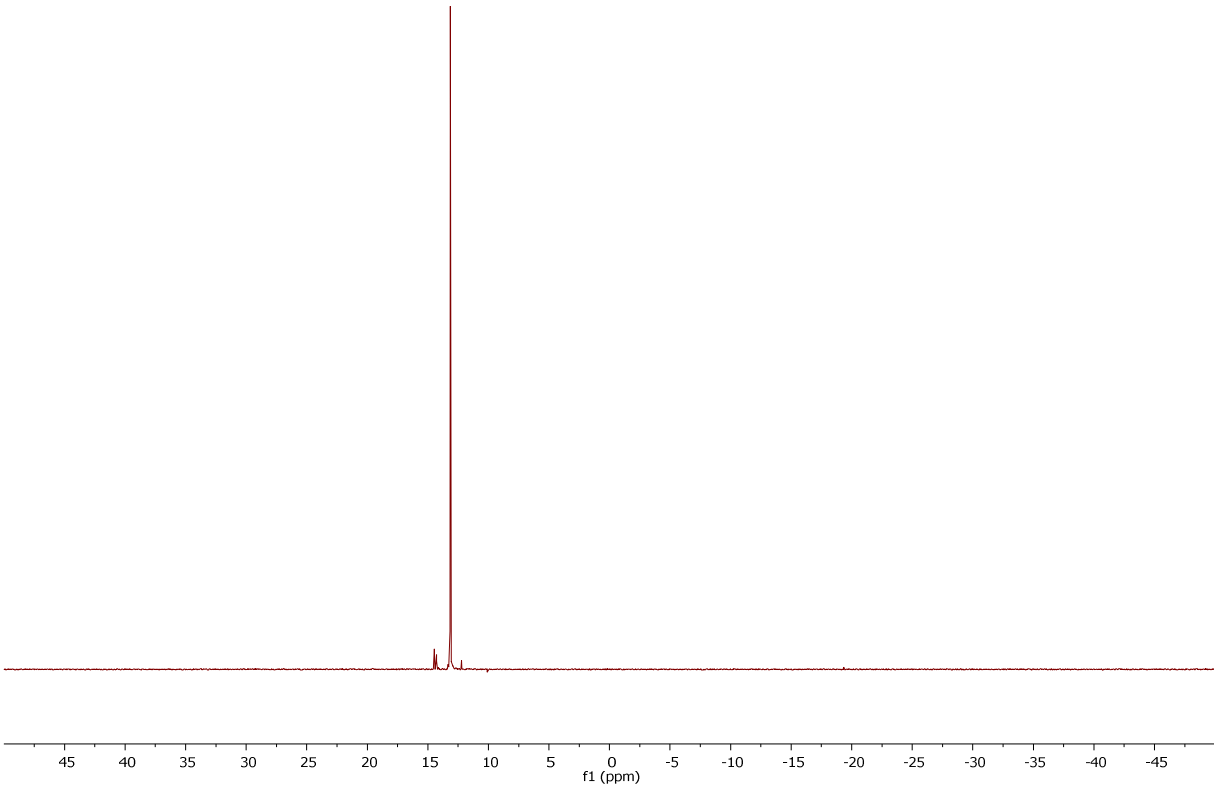

Figure S47. $^{31}P\{^{1}H]$ NMR (162 MHz, $CDCl_3$) spectrum of **18**.

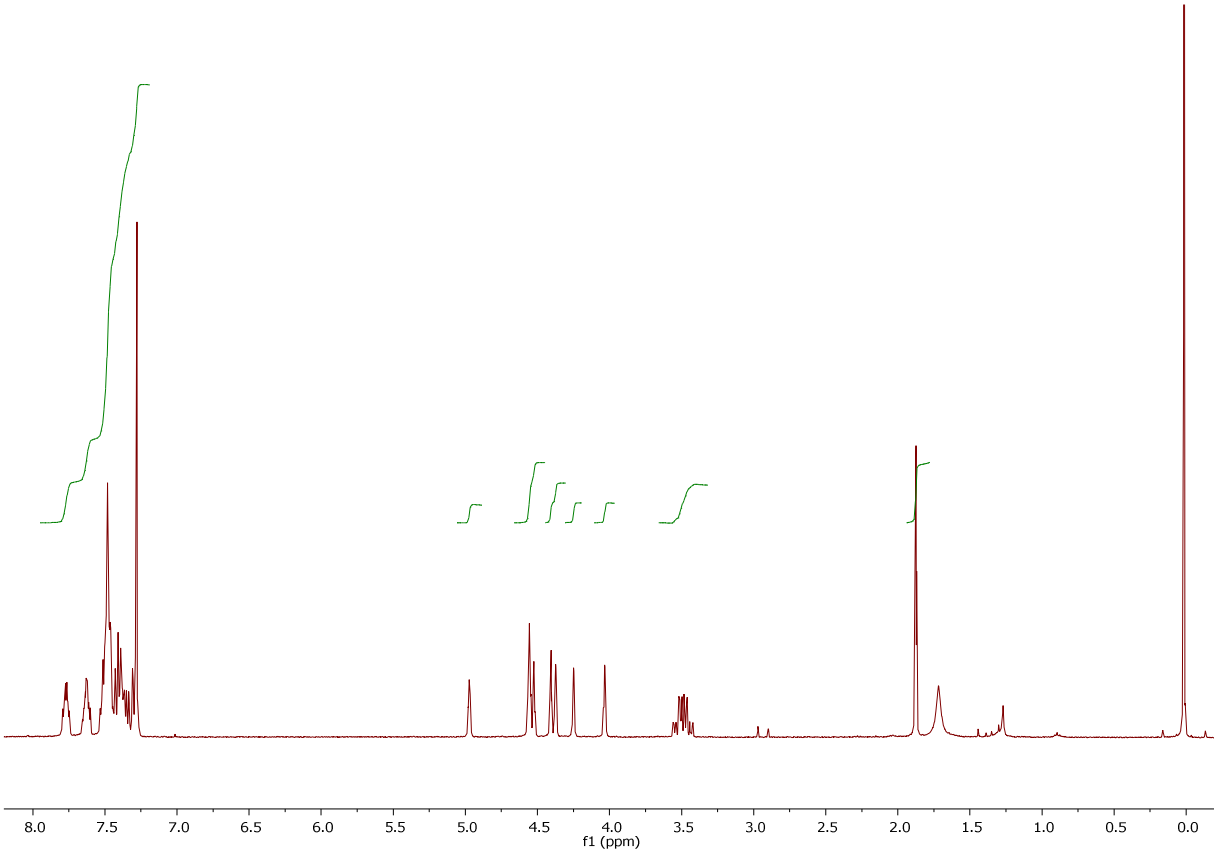

Figure S48. ^{1}H NMR (400 MHz, $CDCl_3$) spectrum of **19**.

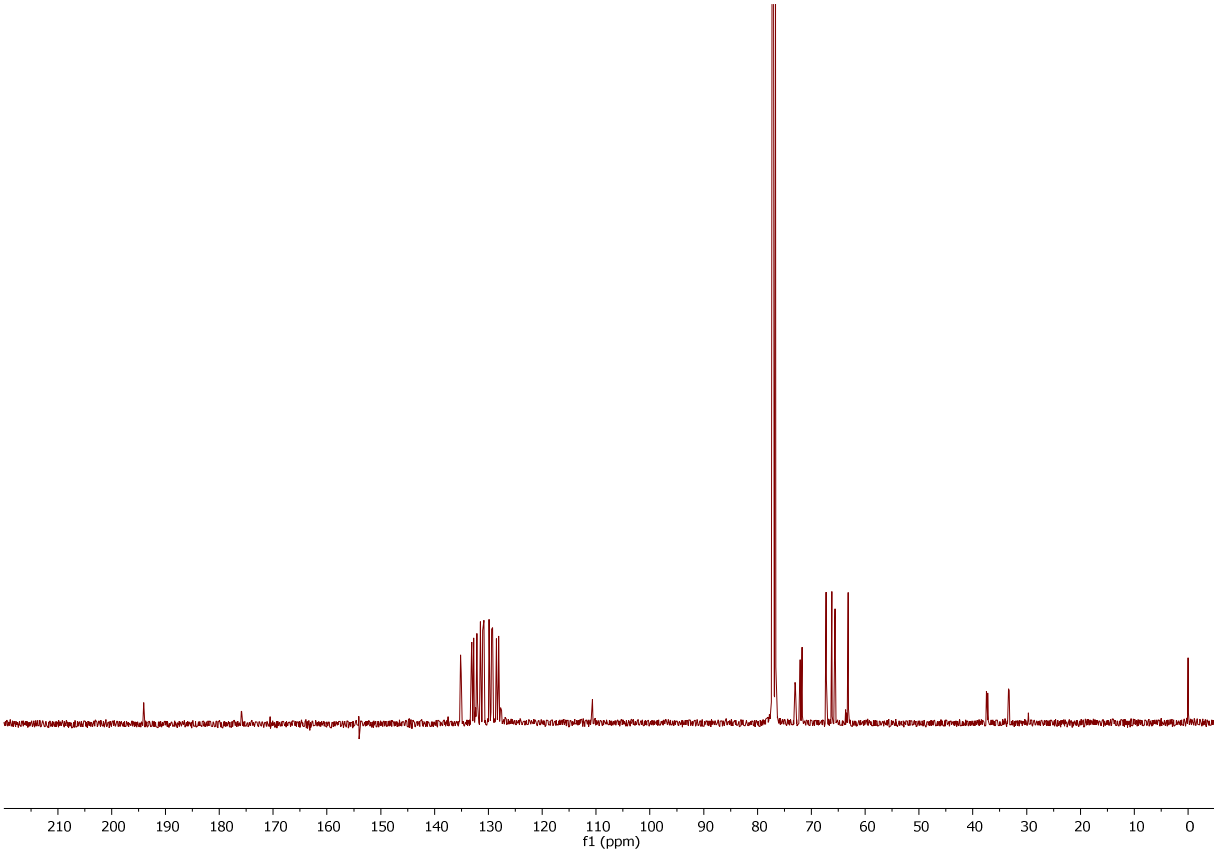

Figure S49. $^{13}C\{^{1}H\}$ NMR (101 MHz, $CDCl_3$) spectrum of **19**.

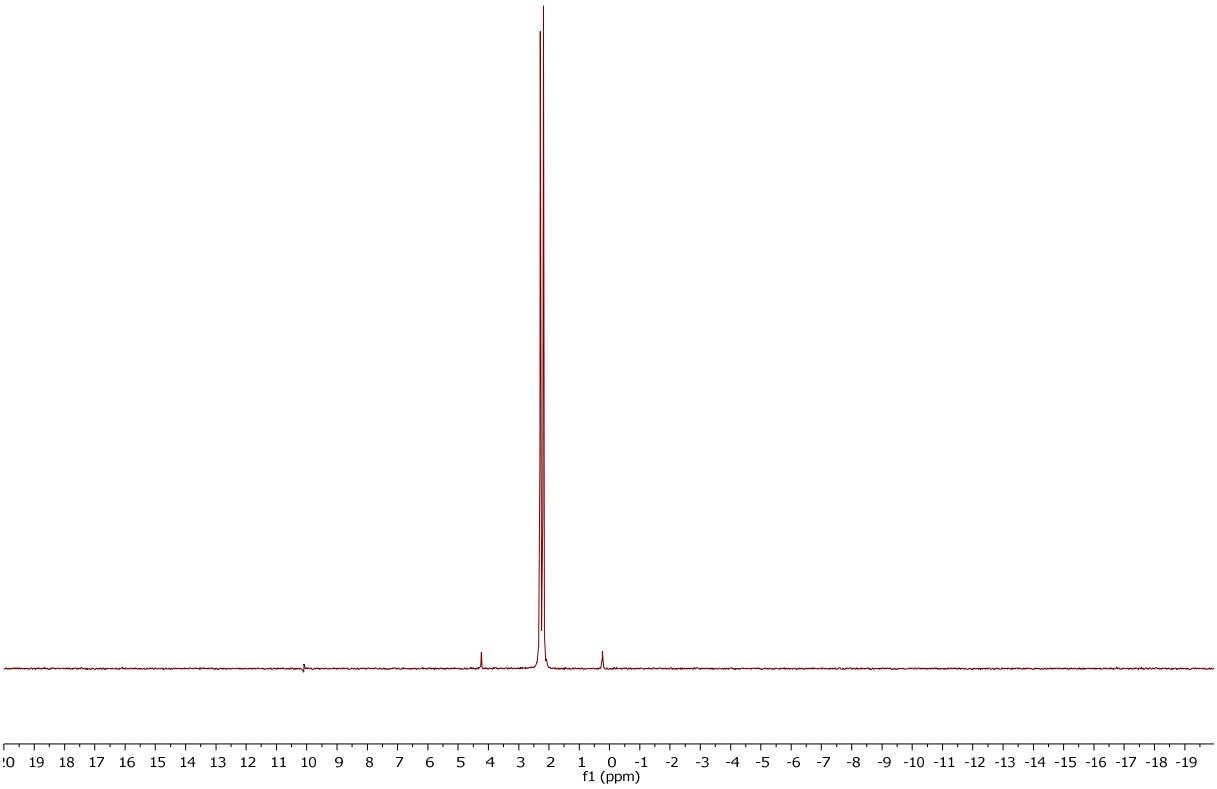

Figure S50. $^{31}P\{^{1}H]$ NMR (162 MHz, $CDCl_3$) spectrum of **19**.

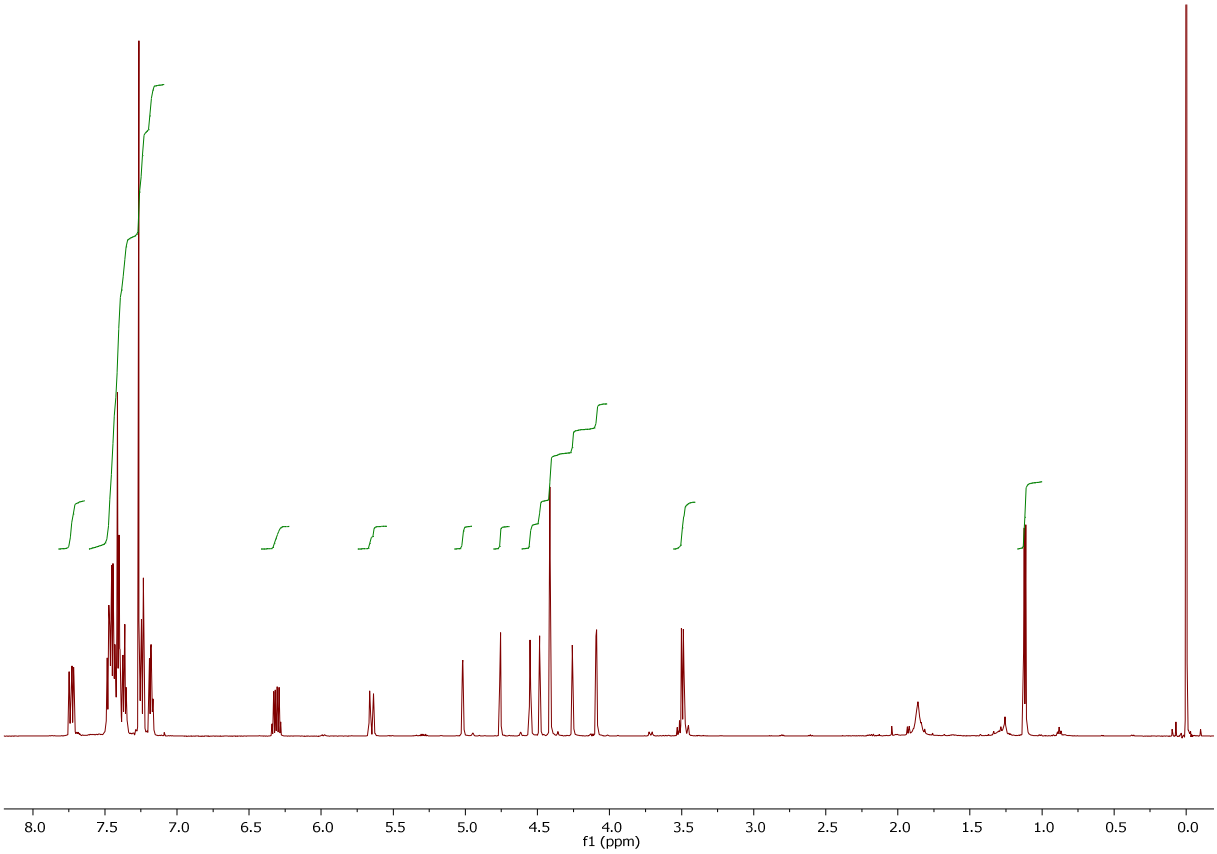

Figure S51. ^{1}H NMR (600 MHz, $CDCl_3$) spectrum of **20**.

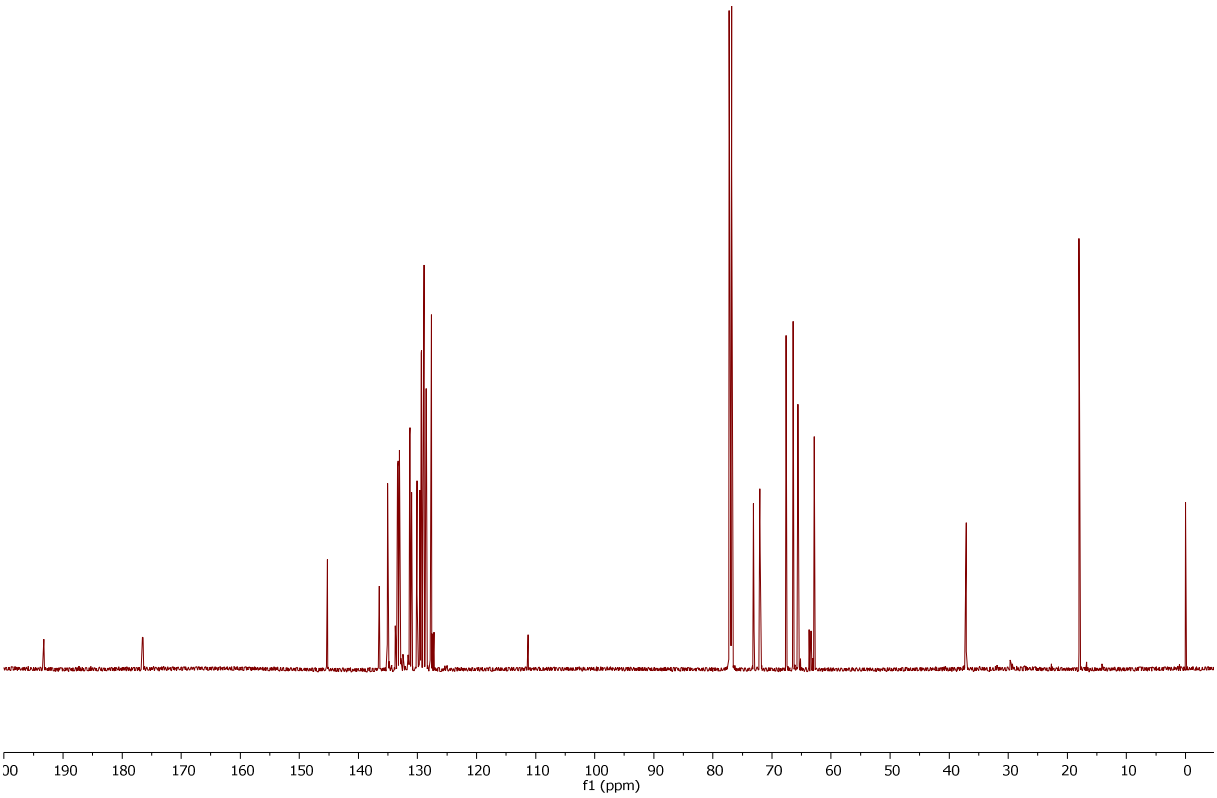

Figure S52. $^{13}C\{^{1}H\}$ NMR (111 MHz, $CDCl_3$) spectrum of **20**.

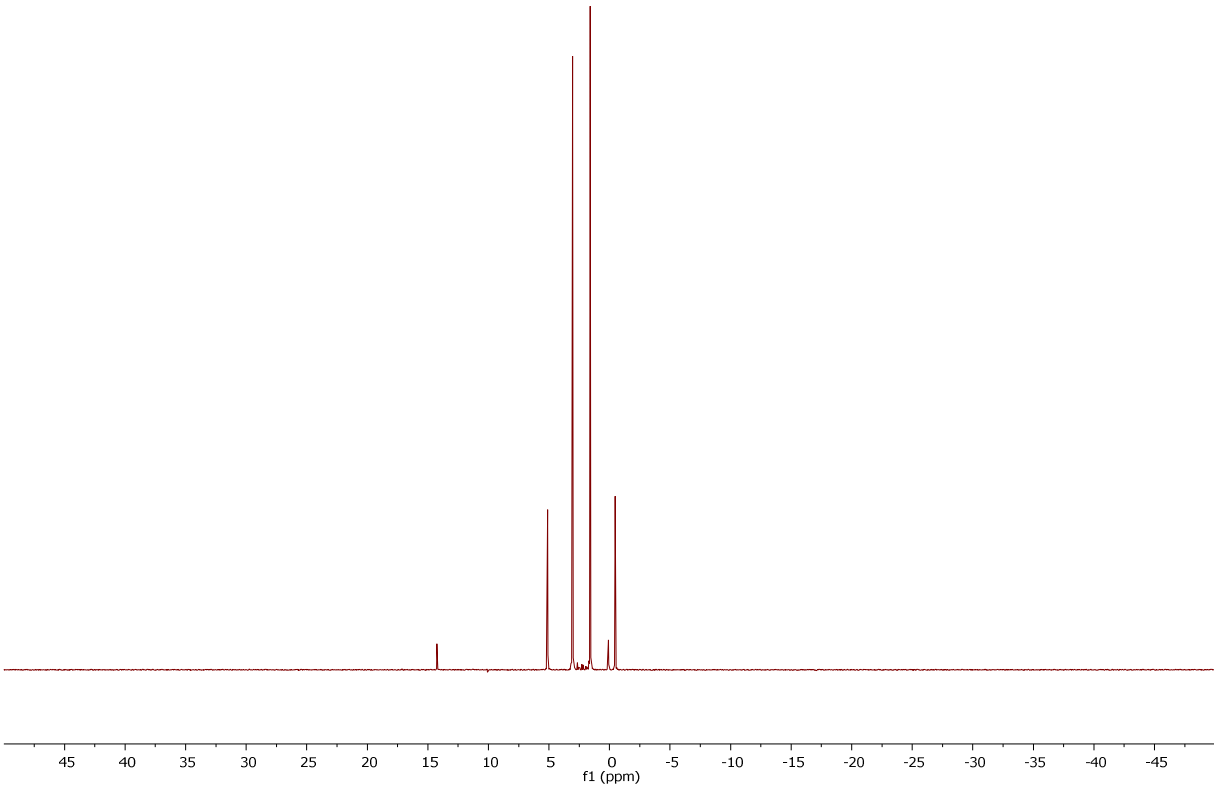

Figure S53. $^{31}P\{^{1}H]$ NMR (162 MHz, $CDCl_3$) spectrum of **20** (peaks at $\delta_P \approx 0.1$ and 14.2 are due to minor impurities present in the bulk sample).

References

1. Sheldrick, G. M. *Acta Crystallogr., Sect. C: Struct. Chem.* **2015**, *71*, 3-8.

2. Sheldrick, G. M. *Acta Crystallogr., Sect. A: Found. Crystallogr.* **2015**, *71*, 3-8.

3. Spek, A. L. *Acta Crystallogr., Sect. C: Struct. Chem.* **2015**, *71*, 9-18.

4. Spek, A. L. *Acta Crystallogr, Sect. D: Biol. Crystallogr.* **2009**, *65*, 148-155.